Soft Matter

PAPER

Cite this: *Soft Matter*, 2017, **13**, 328

Tug-of-war between two elastically coupled molecular motors: a case study on force generation and force balance

Mehmet Can Uçar and Reinhard Lipowsky*

Received 11th August 2016,
Accepted 17th November 2016

DOI: 10.1039/c6sm01853j

www.rsc.org/softmatter

Intracellular transport is performed by molecular motors that pull cargos along cytoskeletal filaments. Many cellular cargos are observed to move bidirectionally, with fast transport in both directions. This behaviour can be understood as a stochastic tug-of-war between two teams of antagonistic motors. The first theoretical model for such a tug-of-war, the Müller–Klumpp–Lipowsky (MKL) model, was based on two simplifying assumptions: (i) both motor teams move with the same velocity in the direction of the stronger team, and (ii) this velocity matching and the associated force balance arise immediately after the rebinding of an unbound motor to the filament. In this study, we extend the MKL model by including an elastic coupling between the antagonistic motors, and by allowing the motors to perform discrete motor steps. Each motor step changes the elastic interaction forces experienced by the motors. In order to elucidate the basic concepts of force balance and force fluctuations, we focus on the simplest case of two antagonistic motors, one kinesin against one dynein. We calculate the probability distribution for the spatial separation of the motors and the dependence of this distribution on the motors' unbinding rate. We also compute the probability distribution for the elastic interaction forces experienced by the motors, which determines the average elastic force $\langle F \rangle$ and the standard deviation of the force fluctuations around this average value. The average force $\langle F \rangle$ is found to decrease monotonically with increasing unbinding rate ε_0. The behaviour of the MKL model is recovered in the limit of small ε_0. In the opposite limit of large ε_0, $\langle F \rangle$ is found to decay to zero as $1/\varepsilon_0$. Finally, we study the limiting case with $\varepsilon_0 = 0$ for which we determine both the force statistics and the time needed to attain the steady state. Our theoretical predictions are accessible to experimental studies of *in vitro* systems consisting of two antagonistic motors attached to a synthetic scaffold or crosslinked *via* DNA hybridization.

1 Introduction

Intracellular cargos such as vesicles and organelles are transported by cytoskeletal motors.[1] Conventional kinesin and cytoplasmic dynein represent two types of cytoskeletal motors that walk along microtubules in opposite directions.[2,3] Many cargos are observed to perform a bidirectional movement on the microtubules with frequent reversals.[4,5] This behaviour reflects the presence of two antagonistic motors, plus-end directed kinesin and minus-end directed dynein, on the same cargo. These motors try to pull the cargo in their preferred direction of motion, thereby performing a stochastic tug-of-war. The first theoretical model for such a stochastic tug-of-war was introduced by Müller, Klumpp, and Lipowsky (MKL)[6–8] and corroborated by the observations of endosome transport in amoebae[9] and fungi.[10]

Max Planck Institute of Colloids and Interfaces, 14476 Potsdam, Germany. E-mail: lipowsky@mpikg.mpg.de

The MKL model was based on two simplifying assumptions: (i) all motors move with the same velocity in the direction of the stronger team and (ii) this matching of the velocities sets in as soon as the cargo is pulled by motors from both teams. Thus, for two antagonistic motors, the MKL tug-of-war state is characterized by the following properties. When both motors are simultaneously bound to the filament, they experience mutual interaction forces which are of equal magnitude and opposite direction, in accordance with Newton's third law. The absolute value of this interaction force, the so-called cargo force F_{ca}, is determined uniquely by the characteristic force–velocity relations of the motors and the condition of velocity-matching under this force.[6,8] The cargo then moves with this generally low, but nonzero velocity v_{ca} in the direction of the stronger motor. In the special case of equally strong motors the cargo is in a stalled state with zero velocity.

In the MKL model, the motion of the motors is described in a coarse-grained manner, averaging over the discrete steps of the individual motors. Here, we extend this model by including

these discrete steps, following the theoretical approach developed in ref. 11 and 12 for two identical motors that pull in the same direction. We consider two antagonistic motors which are coupled to their common cargo *via* two elastic linkers. We then use the force balance between the motors and the cargo to derive an effective elastic coupling between the two motors. With each step taken by one of the motors, the effective linker is either stretched or compressed and an elastic force is induced acting on both motors. The velocity-matching condition can therefore only be reached, in general, after the motors have taken multiple steps.

When the tug-of-war involves antagonistic motor teams consisting of several identical motors, the MKL model makes the additional assumption that the overall load acting on one team is shared equally by all motors in that team. This assumption has been previously criticized to represent a mean-field approximation because it ignores fluctuations in the load sharing.[13–15] In order to examine the latter fluctuations, the authors in ref. 13–15 studied such antagonistic motor teams. In contrast to these previous studies, we focus here on the simplest case of two antagonistic motors for which load sharing does not play any role. On the one hand, the case of 1 + 1 motors is useful in order to elucidate the basic concepts of force balance and force fluctuations. In fact, as shown below, this case already implies a nontrivial force balance, with an average interaction force that depends strongly on the unbinding rate ε_0 of the individual motors and decays to zero for large ε_0. On the other hand, the study of the 1 + 1 motor system allows us to perform a detailed comparison between (i) the tug-of-war of two elastically coupled motors that perform discrete steps and (ii) the tug-of-war of two antagonistic motors as described by the MKL model.

The theoretical results described below can be scrutinized by experimental *in vitro* studies based on recently developed protocols[16–20] to control the number of active motors on synthetic molecular scaffolds. Evidence for a tug-of-war mechanism between kinesin and dynein attached to such scaffolds was observed in ref. 19 and 20. Very recently, it has also been demonstrated that one can directly crosslink a single, fluo-labeled kinesin with a single, fluo-labeled dynein *via* DNA hybridization.[21] For such two-motor constructs, one should be able to measure the probability distribution for the spatial separation of the two motors along the filament and, in this way, directly scrutinize the predictions of our theory. Furthermore, as shown below, the distribution for the motor–motor separation also determines the probability distribution for the elastic interaction forces and, thus, the average elastic force $\langle F \rangle$ between the motors.

This paper is organized as follows. First, we briefly review (i) the single motor description in Section 2.1, thereby introducing the single motor parameters used in our model, and (ii) the cargo force predicted by the MKL model in Section 2.2. Next, the force balance for a tug-of-war between two elastically coupled motors is considered and the associated state space for this process is defined in Section 2.3. We describe the system as a Markov process with (i) several transient states corresponding to different extensions of the effective elastic linker and (ii) two absorbing states defined by a single plus- or minus-end motor bound to the filament. The rates of the network are determined using single motor parameters characterising the stepping and unbinding behaviour. Section 3 reports the results on the steady state probability distributions of 2-motor runs with both motors attached to the filament, the average force experienced by the motors, as well as a detailed study of the limiting case of zero unbinding rates. In the latter case, both the force statistics and the time needed to reach the steady state are determined as a function of the elastic coupling strength.

2 Model

2.1 Single motor description

When a motor binds to the filament, it steps along the filament in a preferred direction. In the absence of an external force F, the motor moves with its zero-force forward velocity towards the preferred end of the filament. We use the convention that a resisting force acting as a load on the motor has a positive sign whereas an assisting force pulling the motor in its preferred stepping direction has a negative sign. This convention is used both for plus-directed and for minus-directed motors. With increasing load force, the motor velocity decreases until the force reaches the motor's stall force F_s at which the motor velocity vanishes. Experimental studies provide strong evidence that the kinesin-1 motor steps backwards for load forces $F > F_s$.[22,23] The explicit form of the force–velocity relation for a single motor can be obtained from fits to experimental data or provided by piecewise linear relations as in previous theoretical studies, see *e.g.* ref. 6, 13 and 15 and Appendix A. Here, we will use a convenient parametrization of the force–velocity relation as introduced in ref. 11 which has the form

$$v(F) = \frac{v_{\max}\frac{v_{\min}-v_0}{v_0-v_{\max}} + v_{\min}\left(\frac{v_{\max}}{v_{\min}}\frac{v_0-v_{\min}}{v_0-v_{\max}}\right)^{F/F_s}}{\frac{v_{\min}-v_0}{v_0-v_{\max}} + \left(\frac{v_{\max}}{v_{\min}}\frac{v_0-v_{\min}}{v_0-v_{\max}}\right)^{F/F_s}}. \quad (2.1)$$

The parameters $v_{\max}$ and $v_{\min}$ determine the limits of $v(F)$ for large negative and large positive values of F, respectively. The zero-force velocity $v(F = 0)$ is given by the parameter v_0. In the following, we use the force–velocity relation in eqn (2.1) for both motors. The parameters v_0, $v_{\max}$, $v_{\min}$ and F_s can be specified in order to obtain close approximations for experimentally determined force–velocity relations, *e.g.* as given in ref. 22 for kinesin-1 and in ref. 24 for cytoplasmic dynein.

Another single motor property that has been measured for kinesin as a function of load force[22,23] is the forward-to-backward stepping ratio q which is defined as the number of forward steps divided by the number of backward steps as observed within a certain time interval. This ratio was found to depend exponentially on the load force and to be well fitted by[22]

$$q(F) = q_0^{1-F/F_s} \quad \text{with } q_0 = 800 \text{ and } F_s = 7 \text{ pN} \quad \text{for kinesin.} \quad (2.2)$$

For dynein, the corresponding parameters have not been measured directly but the single motor data on yeast dynein in ref. 25 and 26 provide the estimates

$$q_0 = 4 \quad \text{and} \quad F_s = 7 \text{ pN} \quad \text{for dynein.} \quad (2.3)$$

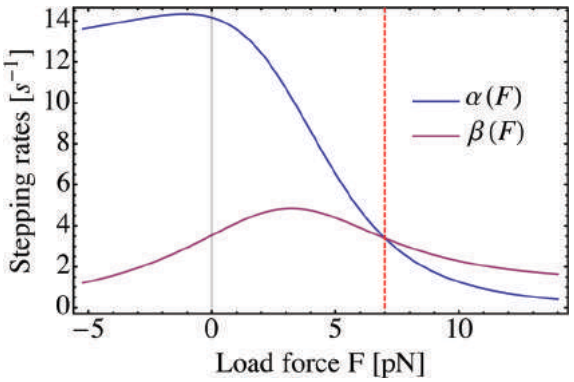

Fig. 1 Forward and backward stepping rates, α and β, as a function of load force F for yeast dynein. The rates are computed *via* eqn (2.4) and (2.5) with the force–velocity relationship $v(F)$ and the step ratio $q(F)$ as given by eqn (2.1) and (2.2), using the single motor parameters in Table 1. The dashed vertical line (red) corresponds to the motor's stall force F_s = 7 pN.

We now use the force–velocity relationship $v(F)$ and the forward-to-backward stepping ratio $q(F)$ together with the step size ℓ to define the forward stepping rate of a single motor by

$$\alpha(F) \equiv \frac{v(F)}{\ell}\frac{q(F)}{q(F)-1} \tag{2.4}$$

and its backward stepping rate by

$$\beta(F) \equiv \frac{v(F)}{\ell}\frac{1}{q(F)-1}, \tag{2.5}$$

which implies $\alpha/\beta = q$ and $\alpha - \beta = \ell v$.[11] The force-dependence of the two stepping rates α and β is illustrated in Fig. 1 for yeast dynein. At the stall force $F = F_s$, the two stepping rates are equal, implying that forward and backward steps are equally likely. For $F > F_s$, backward steps are more likely than forward steps and both stepping rates decay monotonically with increasing force. For $F < F_s$, on the other hand, forward steps are more likely than backward steps but the individual stepping rates are nonmonotonic as a function of F. In fact, the backward stepping rate β for dynein exhibits a pronounced maximum at the load force F = 3.21 pN, arising from the relatively small value q_0 = 4 of the forward-to-backward stepping ratio. For kinesin, on the other hand, which is characterized by a much larger value of q_0, no such maximum of β is found.

A motor bound to a filament unbinds from this filament with a constant unbinding rate in the absence of external forces. We denote this zero-force unbinding rate of a single motor by ε_0. When a force acts on the cargo, the motor-filament bond is more likely to break. Although the unbinding process is very complex on a molecular scale, it can be approximately described as an escape process of a particle in a potential well. According to Kramers' theory,[27] the force-dependence of the motor's unbinding rate is then approximately exponential and given by

$$\varepsilon(F) = \varepsilon_0 \exp(|F|/F_d), \tag{2.6}$$

where F_d is the detachment force, another force scale that characterizes each motor type. Here and below, the force F represents the tangential force component acting parallel to the long axis of the filament, with the previously mentioned sign convention that F is positive when it acts against the preferred stepping direction that the motor has in the absence of force. Note that $\varepsilon(F)$ is taken to depend only on the absolute value $|F|$, and not on the direction of the force which implies that resisting and assisting forces increase the unbinding rate by the same amount. This simplifying assumption is not crucial, however, because, as we will see below, assisting forces are almost never generated by a tug-of-war.

In the following, we use this single motor description for two different types of motors, kinesin and dynein, which represent the best studied examples for processive plus-end and minus-end directed motors. We will use the notation $F_s^{\pm}$ and $F_d^{\pm}$ for the stall and detachment forces of these two motor species. Our sign convention for F implies that both stall and detachment forces are positive. In addition, this convention also implies that a positive force acting on the plus-end directed motor points towards the minus end of the filament whereas a positive force acting on the minus-end directed motor points towards the filament's plus end. Furthermore, because of the opposite directionality, the force–velocity relationships $v^+(F)$ and $v^-(F)$ for the plus- and minus-directed motors have the form $v^+(F) = +v(F)$ and $v^-(F) = -v(F)$ with $v(F)$ as in eqn (2.1).

2.2 Cargo force in the MKL model

Before we consider the tug-of-war between elastically coupled motors, we will first summarize the main properties of the tug-of-war in the MKL model which provides a useful reference process. As described in Appendix A, the latter process is characterized by instantaneous velocity matching between the different motors. The corresponding matching condition can be visualized by plotting the two force–velocity relations for the individual motors in the same (F,v)-diagram.[8] The intersection point of these two relations provides the matching condition for the MKL tug-of-war as illustrated in Fig. 2 for the case in

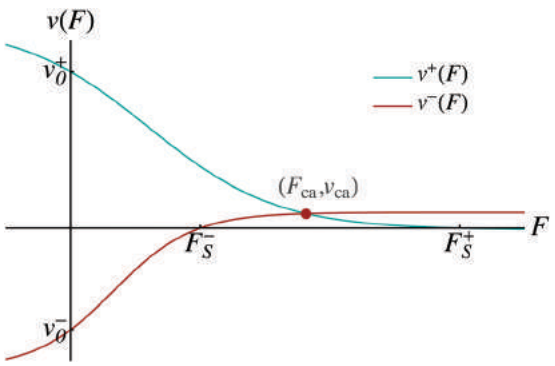

Fig. 2 Matching condition for the velocities of two antagonistic motors as used in the MKL tug-of-war model: force–velocity relations as given by eqn (2.1) for a plus (green) and a minus (red) motor with zero-force velocities $v_0^+ > 0$ and $v_0^- < 0$. The intersection point $(F, v) = (F_{ca}, v_{ca})$ of the two force–velocity relations defines the velocity-matched state in which both motors move with the same velocity v_{ca} and experience the same single motor force as provided by the cargo force $F = F_{ca}$. In this example, the stall force F_s^+ of the plus motor exceeds the stall force F_s^- of the minus motor which implies $v_{ca} > 0$, *i.e.* both the cargo and the two antagonistic motors move towards the plus end of the filament.

which the stall force F_s^+ of the plus motor exceeds the stall force F_s^- of the minus motor.

In general, the intersection point $(F, v) = (F_{ca}, v_{ca})$ of the two force–velocity relations defines the velocity-matched state in which the cargo and the motors move with the same velocity v_{ca} and the two motors experience the same single motor force, namely the cargo force $F = F_{ca}$. The cargo force is always positive because it is located between the stall forces F_s^+ and F_s^- of the two motors, both of which are positive by definition. Thus, according to our sign convention for single motor forces, the cargo force acts as a resisting force on both motors: it represents the absolute value of the two opposing forces that the cargo exerts simultaneously onto the plus and onto the minus motor.

2.3 Elastic coupling between the motors

We now consider one kinesin and one dynein motor pulling on the same cargo particle *via* elastic linkers as illustrated in Fig. 3. We use the Cartesian coordinate x parallel to the filament to describe the positions of the motors and the cargo along this filament. The coordinate x is chosen to increase towards the plus end of the filament. Thus, each motor–cargo configuration is described by the positions x_{ki}, x_{dy}, and x_{ca} with $x_{dy} < x_{ca} < x_{ki}$. Furthermore, to discuss the elastic forces acting between the motors and the cargo, we will first define these forces with respect to the coordinate x which implies that we temporarily use a different sign convention for these interaction forces compared to the single motor forces. Thus, in the following paragraph, the elastic interaction forces are taken to be positive when they point towards the plus end of the filament and negative when they point towards the filament's negative end.

Elastic forces between the cargo and the motors. The linkers between the motors and the cargo are described by harmonic springs with spring constant κ and rest length $L_\parallel$. The kinesin motor then exerts the force

$$F_{ki,ca} = \kappa(x_{ki} - x_{ca} - L_\parallel) \quad (2.7)$$

onto the cargo. Likewise, the dynein motor exerts the force

$$F_{dy,ca} = -\kappa(x_{ca} - x_{dy} - L_\parallel) \quad (2.8)$$

onto the cargo. We now assume that, for given positions x_{ki} and x_{dy}, the elastic forces balance each other on timescales that are short compared to the timescales of the single motor transitions. This elastic force balance implies $F_{ki,ca} + F_{dy,ca} = 0$ and $x_{ca} = \frac{1}{2}(x_{ki} + x_{dy})$. Eliminating the cargo position x_{ca} from the expressions in eqn (2.7) and (2.8), we obtain the forces

$$F_{ki,ca} = \tfrac{1}{2}\kappa(x_{ki} - x_{dy} - 2L_\parallel) = K(x_{ki} - x_{dy} - L_0) \quad (2.9)$$

and

$$F_{dy,ca} = \tfrac{1}{2}\kappa(x_{ki} - x_{dy} - 2L_\parallel) = -K(x_{ki} - x_{dy} - L_0), \quad (2.10)$$

which depend only (i) on the coordinate difference $x_{ki} - x_{dy}$ of the two motor positions and (ii) on the effective spring parameters

$$K \equiv \kappa/2 \text{ and } L_0 = 2L_\parallel. \quad (2.11)$$

Introducing the combined spring extension

$$\Delta L \equiv x_{ki} - x_{dy} - L_0, \quad (2.12)$$

the force that the kinesin exerts on the dynein becomes

$$F_{ki,dy} = F_{ki,ca} = K\Delta L, \quad (2.13)$$

while the force that the dynein exerts on the kinesin has the form

$$F_{dy,ki} = -K\Delta L, \quad (2.14)$$

as required by Newton's third law.

Identification with single motor forces. In order to use the single motor description as described in the previous subsection, we now return to our original sign convention for the force F acting on a single motor. As a consequence, the single motor force is given by

$$F = F_{ki} \equiv -F_{dy,ki} \quad \text{for kinesin,} \quad (2.15)$$

which is positive when the force $F_{dy,ki}$ points towards the minus end of the filament, and by

$$F = F_{dy} \equiv F_{ki,dy} \quad \text{for dynein,} \quad (2.16)$$

which is positive when the force $F_{ki,dy}$ points towards the filament's plus end. Newton's third law as given by $F_{ki,dy} = -F_{dy,ki}$ then assumes the simple form $F_{ki} = F_{dy} = F$.

State space for tug-of-war with elastic coupling. Kinesin and dynein have the same step size $\ell \simeq 8$ nm, see references in Table 1. We further assume that the motor pair can attain a

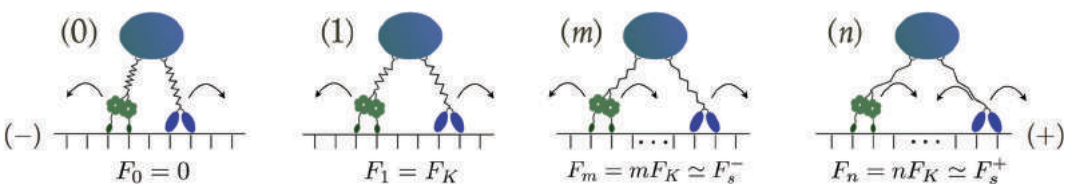

Fig. 3 Different states (j) with j = 0, 1, m and n of two antagonistic motors corresponding to different extensions of the elastic linkers between the motors and the cargo. The kinesin motor (blue "heads") and the dynein motor (green "wheels") prefer to move towards the (+)- and (−)-end of the microtubule, respectively. In state (0), the motor linkers are relaxed and do not generate elastic forces. When the motors perform steps leading to a state (j) with $j > 0$, the spring becomes stretched and generates the elastic force $F_j = jF_K$. As explained in the main text, the single motor forces F_{ki} and F_{dy} acting on kinesin and dynein are defined in such a way that Newton's third law assumes the simple form $F_j = F_{ki} = F_{dy}$. In state (1), for example, both the kinesin and the dynein motor experience the single motor force $F_1 = F_K$. In state (m), the force $F_m = mF_K \simeq F_s^-$, *i.e.* it is comparable to the stall force F_s^- of the minus motor. At this stall force, the minus motor steps forward and backward with equal probability. In state (n), the force F_n is close to the stall force of the plus motor, which can now step forward and backward with (almost) equal probability.

relaxed state with $\Delta L = 0$. It is then convenient to introduce the dimensionless spring extension

$$j = \Delta L/\ell \quad \text{with} \quad -J \le j \le J, \tag{2.17}$$

where $j = J$ represents the maximal stretching and $j = -J$ the maximal compression of the spring.

Each motor behaves as a stochastic stepper with force-dependent forward and backward stepping rates $\alpha(F)$ and $\beta(F)$, as given by eqn (2.4) and (2.5). Following the approach in ref. 11 for two identical motors, we now introduce a discrete state space with states (j) labeled by an integer j with $-J \le j \le J$. Each state (j) corresponds to a certain extension of the elastic spring. We consider two identical motor linkers in series which implies the effective spring constant $K \equiv \kappa/2$ for the elastic coupling between the two motors as in eqn (2.11). When the spring extension is increased by a single motor step with step size ℓ, the elastic force experienced by both motors is increased by the strain force

$$F_K \equiv K\ell = \kappa\ell/2, \tag{2.18}$$

Table 1 Values of the parameters used for kinesin-1 and two types of dynein motors: the values for "strong" and "weak" dynein correspond to yeast and mammalian cells, respectively. A star superscript indicates a parameter for which we did not find experimental data in the literature; the corresponding parameter value was set equal to the experimentally deduced value of another type of motor. For the minimal and maximal velocities of both dynein motors in the force–velocity relationship (2.1) we used the estimated values $v_{\min} \simeq 0.12v_0$ and $v_{\max} \simeq 1.12v_0$, as indicated by the † symbol. For the parameters in this table the strain force is given by $F_K = \kappa l/2 = 0.8$ pN both for kinesin *vs.* strong dynein and for kinesin *vs.* weak dynein

Parameter	Kinesin-1	"Strong" dynein	"Weak" dynein
Zero-force unbinding rate ε_0 [s^{-1}]	1^{35}	1*	1^{36}
Stall force F_s [pN]	7^{22}	$7^{24,26}$	$1.1^{37,38}$
Detachment force F_d [pN]	3.6^{39}	3.3^{40}	3.3*
Linker stiffness κ [pN nm^{-1}]	0.2^{17}	0.2*	0.2*
Step size l [nm]	$8^{17,22}$	8^{25}	8^{24}
Zero-force step ratio q_0	800^{22}	4^{25}	4*
Zero-force velocity v_0 [nm s^{-1}]	547^{11}	85^{25}	800^{24}
Backward velocity $v_{\min}$ [nm s^{-1}]	12^{11}	$10^{\dagger}$	$100^{\dagger}$
Max. velocity $v_{\max}$ [nm s^{-1}]	573^{11}	$100^{\dagger}$	$900^{\dagger}$

see Fig. 3. The elastic force acting between the motors is then given by

$$F_j \equiv jF_K \quad \text{in state } (j). \tag{2.19}$$

When one of the motors performs a step, the elastic force acting between the two motors changes monotonically from its initial value before the step to its final value after the step. As a consequence, the effective force acting during the stretching transition from (j) to $(j+1)$ is given by

$$\bar{F}_{j>} = (F_j + F_{j+1})/2 = F_K(j + 1/2), \tag{2.20}$$

i.e. by the arithmetic mean of the forces acting before and after such a step.[28] Likewise, the effective force acting during the compression transition from (j) to $(j-1)$ has the form

$$\bar{F}_{j<} = (F_j + F_{j-1})/2 = F_K(j - 1/2). \tag{2.21}$$

Motor kinetics and transition rates. The dynamics of the two-motor runs can be investigated by considering the stochastic process on the discrete state space corresponding to the "stretching" or "compression" of the effective spring between the motors. In state (0) the spring is relaxed. If one of the motors performs a single step, the elastic spring of the two-motor system can be stretched or compressed by $\ell/2$ and the system undergoes a transition to states (1) or (−1), respectively, see the network representation in Fig. 4. In general, the motor system undergoes a forward transition from state (j) to state $(j+1)$ if kinesin or dynein performs a forward step. The corresponding stepping rates are given by $\alpha^{\pm}(\bar{F}_{j>})$ for the individual motors which implies the forward rate

$$\omega_f(j) = \alpha^{+}(\bar{F}_{j>}) + \alpha^{-}(\bar{F}_{j>}) \quad \text{for } (j) \to (j+1) \tag{2.22}$$

with $-J \le j \le J$ and the boundary condition $\omega_f(J) = 0$, see Fig. 4. Each forward transition leads to an increased stretching or a reduced compression of the elastic coupling between the two motors.

Likewise, the motor system undergoes a backward transition from state (j) to state $(j-1)$ if kinesin or dynein performs a

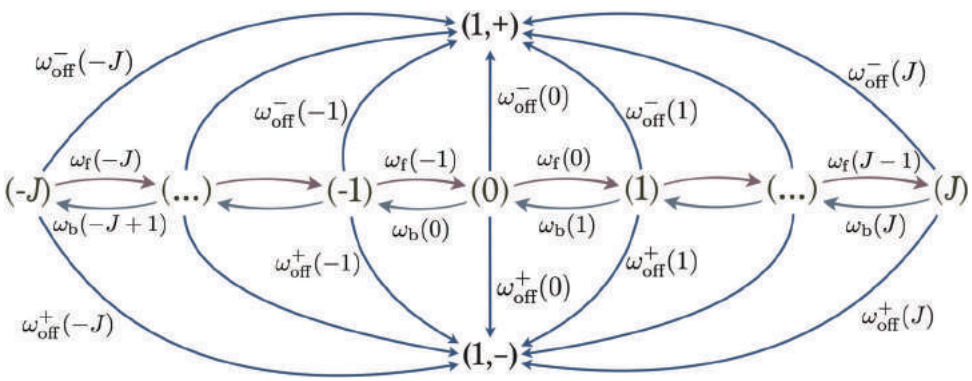

Fig. 4 State space associated with different states of the elastic linker. The two states (1, +) and (1, −) are the absorbing states with a single plus and minus motor bound to the microtubule. States labelled by integer j with $-J \le j \le J$ denote the states with a stretched and compressed linker for $j > 0$ and $j < 0$, respectively. Starting from state (j), the plus and minus motors unbind from the filament with rates $\omega_{off}^{+}(j)$ and $\omega_{off}^{-}(j)$. Furthermore, the motors undergo a forward transition from (j) to $(j+1)$ with rate $\omega_f(j)$ and a backward transition from (j) to $(j-1)$ with rate $\omega_b(j)$.

backward step. The corresponding stepping rates are given by $\beta^{\pm}(\bar{F}_{j>})$ for the individual motors which implies the backward rate

$$\omega_b(j) = \beta^{+}(\bar{F}_{j<}) + \beta^{-}(\bar{F}_{j<}) \quad \text{for } (j) \rightarrow (j-1) \quad (2.23)$$

with $-J \leq j \leq J$ and the boundary condition $\omega_b(-J) = 0$, see Fig. 4. Each backward transition leads to a reduced stretching or an increased compression of the elastic coupling between the two motors.

In state (j), each of the motors can unbind (or detach) from the filament. The corresponding unbinding rates have the form

$$\varepsilon^{\pm}(F_j) = \varepsilon_0^{\pm}\exp(|F_j|/F_d^{\pm}) \equiv \omega_{off}^{\pm}(j) \quad (2.24)$$

for the two types of motors. The overall unbinding rate from state (j) is then given by

$$\omega_{off}(j) = \omega_{off}^{+}(j) + \omega_{off}^{-}(j). \quad (2.25)$$

Motor parameters. In the following, we will study the tug-of-war between one plus-directed motor and one minus-directed motor. Most single motor parameters will be kept fixed and assume values as appropriate for kinesin-1 and strong dynein, see Table 1. One parameter that we will vary systematically is the zero-force unbinding rate

$$\varepsilon_0 \equiv \varepsilon_0^{+} = \varepsilon_0^{-}. \quad (2.26)$$

As we will see, the elastically coupled tug-of-war is characterized, in the limit of small ε_0, by essentially the same force balance as the MKL tug-of-war. Another parameter of the motor system that will be varied systematically is the elastic coupling between the two motors as described by the strain force $F_K = K\ell = \kappa\ell/2$. In order to ensure that the finite size of the state space does not affect our results, we will always use a sufficiently large state space with $(2J+1) \geq 101$.

3 Results

3.1 Steady state properties of tug-of-war

The elastic coupling between the two antagonistic motors is only effective as long as both motors are attached to the filament and perform a 2-motor run. The latter runs are described by transitions between the states (j) in Fig. 4 and are terminated as soon as one of the motors unbinds from the filament. After such an unbinding event, the cargo is bound to the filament by a single motor as described by the states $(1, +)$ and $(1, -)$ in Fig. 4. These 1-motor runs continue until the unbound motor rebinds to the filament. We will assume that the rebinding typically leads to the state (0) which is relaxed in the sense that the two motors do not experience elastic interaction forces. Thus, after rebinding, a new 2-motor run starts from the initial state (0).

As described previously for the 2-motor runs of two identical motors,[11,12] the steady state probability distribution as obtained from an ensemble average over many 2-motor runs can be replaced by a time average over a concatenated 2-motor run that is obtained by redirecting all transitions to the absorbing states towards a certain initial state. For the network depicted in Fig. 4, the absorbing states are provided by $(1, +)$ and $(1, -)$ and the initial state is taken to be the relaxed state (0). As a result, we obtain the redefined network in Fig. 12 which has no absorbing states. The corresponding steady state probability distribution can then be calculated by solving the master equation for the redefined network, see Appendix B.

The steady state probability distribution p_j^{st} describes the frequencies with which the effective elastic spring between the two motors has the extension j. The latter extension determines the spatial separation

$$L \equiv L_0 + j\ell \quad (3.1)$$

of the two motors along the filament. The average motor–motor separation is then given by

$$\langle L \rangle = L_0 + \langle j \rangle \ell = L_0 + \ell \sum_{j \neq 0} p_j^{st} j. \quad (3.2)$$

The fluctuating motor–motor separation L should be directly accessible to experimental studies when one combines the recently introduced crosslinking of one fluo-labeled kinesin and one fluo-labeled dynein *via* DNA hybridization[21] with advanced methods of fluorescence imaging such as FIONA.[29]

In Fig. 5(a) we plot p_j^{st} for different values of the zero-force unbinding rate ε_0. We see that for low unbinding rates, *e.g.* $\varepsilon_0 = 0.01\ s^{-1}$, the probability distribution p_j^{st} shifts towards states with larger j-values. Because the elastic force F_j corresponding to spring extension j is given by $F_j = jF_K$, we can transform the occupation probabilities of the states into the corresponding force distribution by a change of variables from j to F_j, see Fig. 5(b). As shown in the latter figure, a decrease in the unbinding rate leads to a shift of the force distribution towards higher force values and to an average elastic force

$$\langle F \rangle = \sum_j p_j^{st} F_j = F_K \sum_{j \neq 0} p_j^{st} j = F_K[\langle L \rangle - L_0]/\ell \quad (3.3)$$

that approaches the cargo force $F_{ca} = 7$ pN as obtained for velocity-matching. For higher unbinding rates, the occupation probabilities are shifted towards lower j-values, leading to a reduced motor–motor separation and indicating that the motors are likely to unbind from the filament before reaching a state with velocity matching. The relationship in (3.3) implies that the average elastic force $\langle F \rangle$ can be determined from the average motor–motor separation $\langle L \rangle$.

3.2 Dependence of average elastic force on the unbinding rate

For two antagonistic motors coupled by an effective spring as studied here, the elastic interaction forces fluctuate and lead to steady state force distributions as shown in Fig. 5(b) for different values of the unbinding rate ε_0. In contrast, for the MKL model, the mutual interaction force is given by the constant cargo force F_{ca} as obtained *via* velocity matching, see Fig. 2. Inspection of Fig. 5(b) shows that the cargo force F_{ca} provides a better approximation to the average elastic force $\langle F \rangle$ if the unbinding rate becomes smaller. To further examine the relationship between the fluctuating elastic forces and the cargo force,

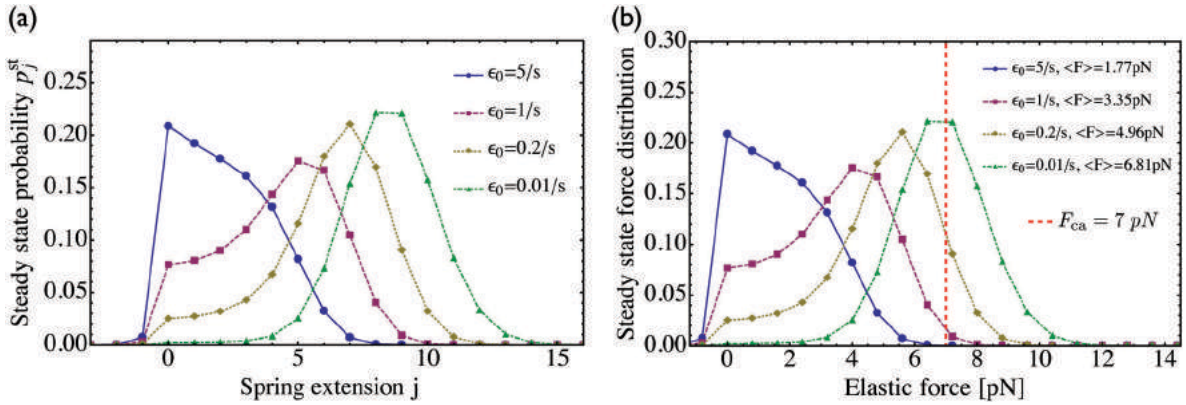

Fig. 5 (a) Steady state probability distributions p_j^{st} for different values of the unbinding rate ε_0 as given in the inset. The spring extension j determines the spatial separation of the two motors *via* $L_0 + j\ell$. Apart from ε_0, all parameters have the values as given in Table 1 for kinesin and strong dynein, which implies the strain force F_K = 0.8 pN; and (b) steady state distributions for the elastic forces as obtained from p_j^{st} by a change of variables from j to $F_j = jF_K$. The dashed vertical line (red) represents the cargo force F_{ca} of the velocity-matched model. For low unbinding rates ε_0, the average elastic force approaches this cargo force. For larger values of ε_0, the force distribution becomes broader and shifts towards lower force values. As a consequence, the average elastic force $\langle F\rangle$ becomes smaller than the cargo force F_{ca}, see average force values in the inset. Likewise, the average spatial separation $L_0 + \langle j\rangle\ell$ of the two motors decreases with increasing unbinding rate ε_0 as follows from the distributions p_j^{st} in (a).

we now consider the very low unbinding rate $\varepsilon_0 = 10^{-5}\ s^{-1}$ and calculate the corresponding steady state probability distribution p_j^{st}. This distribution and the associated force distribution are displayed in Fig. 6 for different values of the strain force F_K. Both for kinesin *vs.* strong dynein as depicted in Fig. 6(a1 and a2), and for kinesin *vs.* weak dynein in Fig. 6(b1 and b2), the cargo force F_{ca} provides a more accurate approximation to the average elastic force $\langle F\rangle$ for smaller values of the strain force F_K. This behaviour arises because smaller F_K-values imply smaller changes in the elastic force induced by single motor

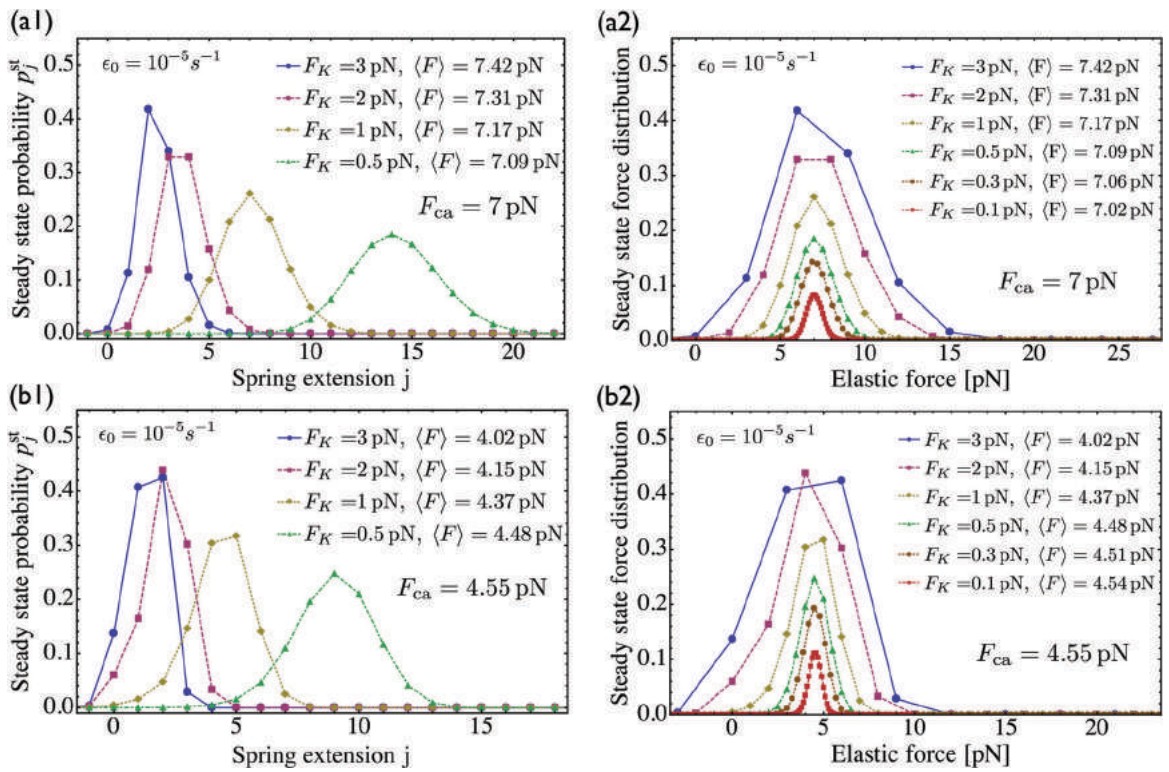

Fig. 6 Steady state probability distributions and force distributions for the small unbinding rate $\varepsilon_0 = 10^{-5}\ s^{-1}$ and for different choices of the strain force F_K: (a1 and a2) kinesin against *strong* dynein, see the motor parameters in Table 1. As we decrease F_K, the average force $\langle F\rangle$ approaches the cargo force F_{ca} = 7 pN more accurately; and (b1 and b2) kinesin against *weak* dynein, see again Table 1. The cargo force now has the lower value F_{ca} = 4.55 pN compared to the kinesin *vs.* strong dynein case in (a). Accordingly, the state (0) in (b1) has a higher occupation probability than the same state in (a1), and the probability for the force value F_0 = 0 is increased in (b2) compared to (a2).

steps which lead to a larger number of accessible force values and, thus, to a smoother interpolation of the discrete force distributions. In addition, the smaller cargo force for the tug-of-war between kinesin and weak dynein compared to kinesin and strong dynein implies that the force value $F_0 = 0$ has a higher probability for the weak dynein case, see Fig. 6.

As shown in Fig. 5, increasing the unbinding rate ε_0 leads to a reduction in the average elastic force $\langle F\rangle$ induced by the motors. This unbinding rate dependence of the average elastic force is displayed in more detail in Fig. 7(a) for different choices of the strain force F_K, with Fig. 7(b) magnifying the limit of small ε_0. In this limit, the deviation of the average elastic force $\langle F\rangle$ from the cargo force F_{ca} increases for larger values of F_K. The decrease of the average force $\langle F\rangle$ with increasing unbinding rate ε_0 is caused by the increasing probability that one of the motors unbinds from the filament before the motors have matched their velocities in the 2-motor run and, thus, before the motors can generate forces comparable to the cargo force F_{ca}. The double-logarithmic plot in Fig. 7(c) reveals that the average elastic force $\langle F\rangle$ decays to zero for large ε_0. It follows from eqn (3.3) that the asymptotic behavior of $\langle F\rangle$ for large ε_0 is determined by the asymptotic behavior of the steady state probability distribution p_j^{st} for large ε_0. The latter behavior can be directly obtained from the master equations (B.1)–(B.4). One then finds from the local flux balance in the states (j) that

$$p_j^{st} \approx p_{j-1}^{st}\frac{\omega_f(j-1)}{\omega_{off}(j)} \quad \text{for } 1 \le j \le J \tag{3.4}$$

and

$$p_j^{st} \approx p_{j+1}^{st}\frac{\omega_b(j+1)}{\omega_{off}(j)} \quad \text{for } -J \le j \le -1 \tag{3.5}$$

in the limit of large unbinding rates $\omega_{off}(j) \sim \varepsilon_0$. Iterating these relations and imposing the normalization condition (B.5), one obtains the asymptotic behavior

$$p_1^{st} \approx \frac{\omega_f(0)}{\omega_{off}(1)} \sim \frac{1}{\varepsilon_0} \quad \text{and} \quad p_{-1}^{st} \approx \frac{\omega_b(0)}{\omega_{off}(-1)} \sim \frac{1}{\varepsilon_0} \quad \text{for large } \varepsilon_0 \tag{3.6}$$

as well as

$$p_0^{st} \approx 1 - p_1^{st} - p_{-1}^{st} = 1 + \mathcal{O}(1/\varepsilon_0) \quad \text{for large } \varepsilon_0 \tag{3.7}$$

whereas all other p_j^{st} are of higher order in $1/\varepsilon_0$. The average elastic force $\langle F\rangle$ as given by (3.3) then behaves as

$$\langle F\rangle \approx F_K(p_1^{st} - p_{-1}^{st}) \sim 1/\varepsilon_0 \quad \text{for large } \varepsilon_0. \tag{3.8}$$

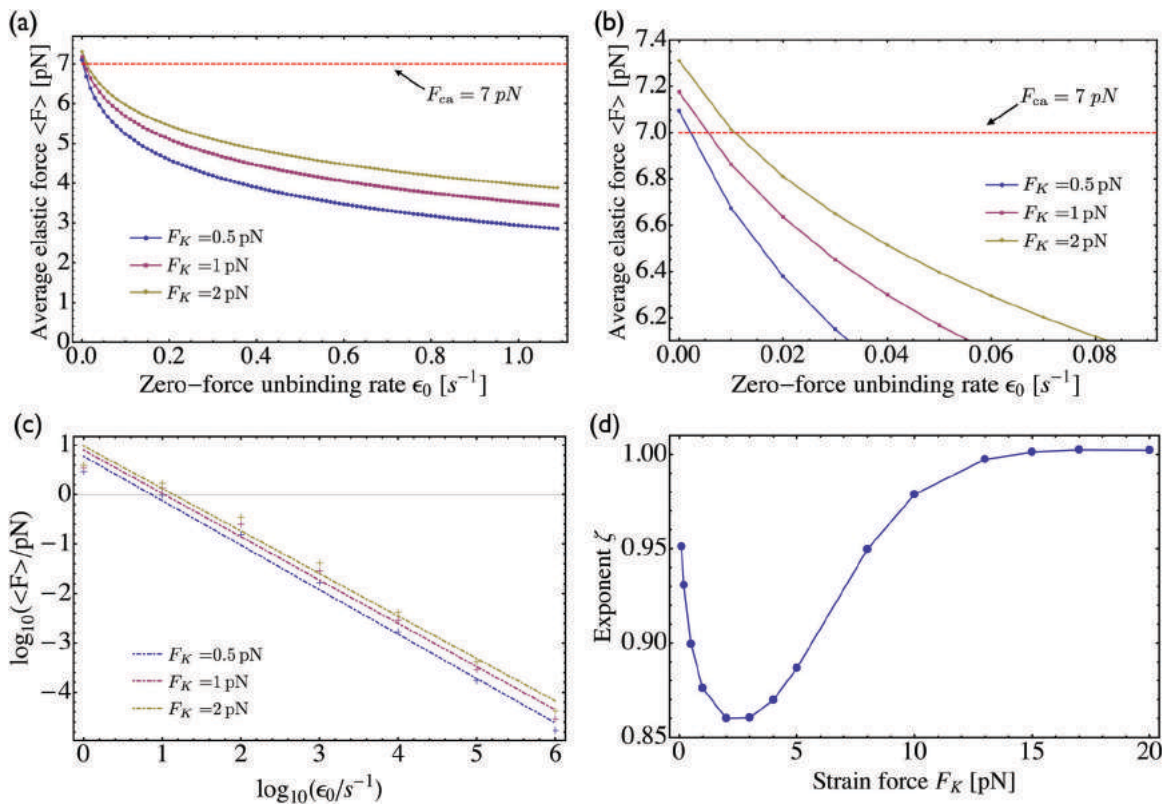

Fig. 7 (a) Average elastic force $\langle F\rangle$ acting on the motors as a function of the zero-force unbinding rate ε_0 for different values of the strain force F_K. The average force $\langle F\rangle$ decreases with increasing ε_0, irrespective of the value for F_K; (b) limiting behaviour of the average elastic force $\langle F\rangle$ for small unbinding rate ε_0. In this limit, the average force $\langle F\rangle$ approaches an asymptotic value $\langle F\rangle_0$ close to the cargo force F_{ca} and the deviation $\langle F\rangle_0 - F_{ca}$ decreases with decreasing F_K; (c) double-logarithmic plot of the average force $\langle F\rangle$ *versus* the unbinding rate which now varies over six orders of magnitude. The straight lines clearly demonstrate that $\langle F\rangle$ decays to zero for large ε_0 and that this decay can be well fitted, over the accessible range of ε_0-values, by a power law of the form $\langle F\rangle \sim 1/\varepsilon_0^{\zeta}$ with the effective decay exponent ζ; and (d) effective exponent ζ as obtained by fitting the data in (c) for different values of the strain force F_K.

The power law behavior $\langle F\rangle \sim 1/\varepsilon_0$ is corroborated by the numerical data in Fig. 7(c) which are well fitted, over the accessible range of ε_0-values as given by $1\ s^{-1} \le \varepsilon_0 \le 10^6\ s^{-1}$, by a power-law of the form $\langle F\rangle \sim 1/\varepsilon^{\zeta}$ with the effective decay exponent ζ. As shown in Fig. 7(d), the effective exponent ζ is found to depend weakly on the strain force F_K for $F_K < 13$ pN and to approach the true asymptotic value $\zeta = 1$ for $F_K > 13$ pN.

3.3 Statistics of elastic forces for vanishing unbinding rate

We now look at the properties of the tug-of-war in the limit in which the two motors can no longer unbind from the filament, corresponding to zero-force unbinding rate $\varepsilon_0 = 0$ which implies that $\omega_{\rm off}(j) = 0$ for all j. In this case, the state space for the tug-of-war between the two motors is reduced to the states $j = -J,\ldots,+J$. For this reduced state space, the probability distribution $p_j(t)$, which starts from the initial distribution $p_j(0) = \delta_{j0}$ at time $t = 0$, evolves towards a steady state distribution $p_j^{\rm st}$ as shown in Fig. 8. The maximum of $p_j^{\rm st}$ is located close to the state $(j = 9)$ characterized by the elastic force $9F_K = 7.2$ pN induced by the effective spring, while the cargo force obtained from velocity matching is $F_{\rm ca} = 7$ pN.

The average elastic force $\langle F\rangle$ for the process with vanishing unbinding rate is shown in Fig. 9 for different values of the strain force F_K. We observe that, regardless of the choice of F_K, the average force $\langle F\rangle$ remains close to the cargo force $F_{\rm ca}$ whereas its standard deviation σ_F increases with increasing F_K. In the limit of small strain forces F_K, the average force $\langle F\rangle$ approaches the cargo force $F_{\rm ca}$ more accurately, in accordance with our previous results. As shown in the right inset of Fig. 9, the standard deviation

$$\sigma_F \equiv \sqrt{\sum_j p_j^{\rm st}\left(F_j^2 - \langle F\rangle^2\right)} \tag{3.9}$$

of the elastic force behaves as

$$\sigma_F \sim \sqrt{F_K} \tag{3.10}$$

over the whole range of F_K-values considered here. For $F_K = 1$ pN and $\varepsilon_0 = 0$, the standard deviation is $\sigma_F \simeq 1.5$ pN. Increasing the zero-force unbinding rate ε_0 for fixed $F_{\rm K} = 1$ pN, the full network in Fig. 4 leads to a slight increase in the deviation σ_F, which then saturates at $\sigma_F \simeq 1.9$ pN for an unbinding rate of $\varepsilon_0 = 1\ s^{-1}$ (data not shown here).

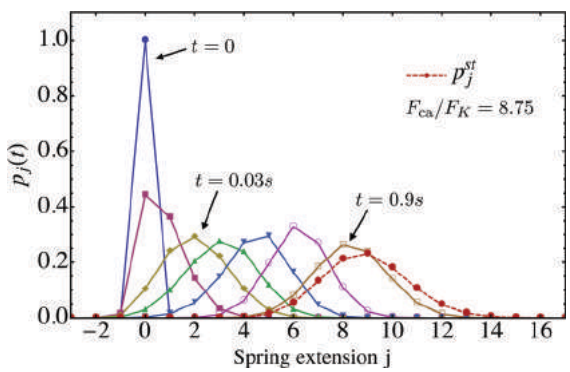

Fig. 8 Time evolution of the probability distribution $p_j(t)$ for unbinding rate $\varepsilon_0 = 0$ and strain force $F_K = 0.8$ pN, the latter parameter being appropriate for strong dynein. The initial probability distribution at time $t = 0$ is given by $p_j(0) = \delta_{j0}$ corresponding to a relaxed spring with zero extension. As t increases, the distribution $p_j(t)$ approaches the steady state distribution $p_j^{\rm st}$ as indicated by the dashed red line.

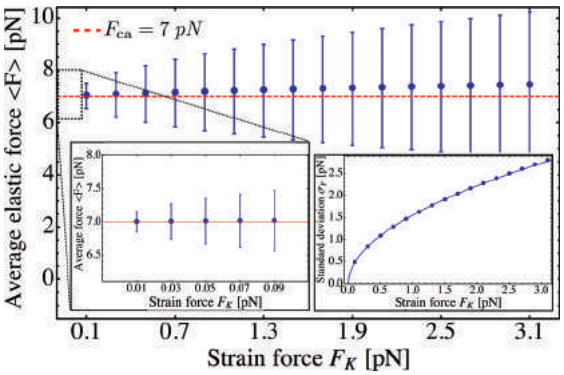

Fig. 9 Average elastic force $\langle F\rangle$ as a function of strain force F_K for unbinding rate $\varepsilon_0 = 0$: the average force $\langle F\rangle$ is roughly independent of F_K for $F_K < 3$ pN and remains close to the cargo force value $F_{\rm ca} = 7$ pN. (left inset) Average force $\langle F\rangle$ for 0.01 pN $\le F_K \le$ 0.09 pN. (right inset) The standard deviation σ_F of the elastic force is proportional to $\sqrt{F_K}$ (solid blue line).

Using these results for the statistics of the elastic forces, we can directly conclude that the average spring extension $\langle j\rangle$ behaves as

$$\langle j\rangle = \langle F\rangle/F_K \simeq F_{\rm ca}/F_K \tag{3.11}$$

and its standard deviation

$$\sigma_j \equiv \sqrt{\sum_j p_j^{\rm st}(j^2 - \langle j\rangle^2)} = \sigma_F/F_K \tag{3.12}$$

as

$$\sigma_j \sim \sqrt{F_K}\Big/F_K = 1\Big/\sqrt{F_K} \sim 1\Big/\sqrt{K}. \tag{3.13}$$

These dependencies on the strain force F_K are displayed in Fig. 10.

The average spring extension $\langle j\rangle$ implies that the two motors have the average separation $\langle \Delta L\rangle = \ell\langle j\rangle$. Thus, we conclude that, in the limit of small F_K corresponding to weakly coupled motors, the average separation between the motors increases as $1/\sqrt{F_K} \sim 1/\sqrt{K}$. Furthermore, the behavior of the standard deviation σ_j is consistent with a Gaussian probability distribution of the form

$$p_j^{\rm st} \propto \exp[-cK(j - \langle j\rangle)^2] \tag{3.14}$$

for the spring extension j where c is a proportionality factor.

It is instructive to compare the distribution as given by (3.14), which arises from the stochastic nature of the tug-of-war and the underlying motor activity, with the equilibrium distribution

$$p_j^{\rm eq} \propto \exp[-\tfrac{1}{2}Kj^2/(k_{\rm B}T)] \tag{3.15}$$

corresponding to thermal fluctuations in the harmonic spring potential $\frac{1}{2}Kj^2$. Comparing the two distributions in (3.14) and (3.15), we can draw two conclusions. First, the motor activity

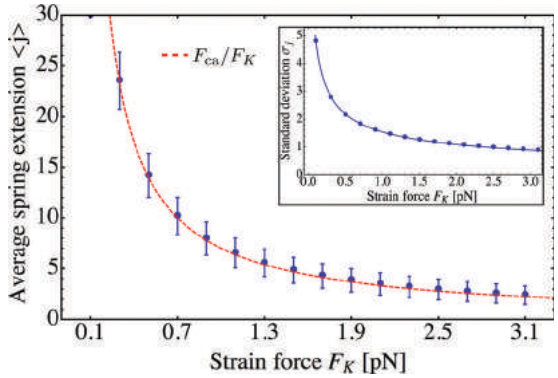

Fig. 10 Average spring extension $\langle j\rangle$ and standard deviation σ_j of these extensions as a function of strain force F_K for unbinding rate $\varepsilon_0 = 0$. Both $\langle j\rangle$ and σ_j decrease with increasing F_K. The F_K-dependence of $\langle j\rangle$ is very well described by F_{ca}/F_K (dashed red line). The standard deviation σ_j is proportional to $1/\sqrt{F_K}$ (full blue line in the inset). This behavior is intimately related to the behavior of the average force $\langle F\rangle$ and the associated standard deviation σ_F, see the main text.

leads to a nonzero average value $\langle j\rangle$ of the spring extension implying a nonzero average separation $\langle \Delta L\rangle = \ell\langle j\rangle$ of the motors and a nonzero average force $\langle F\rangle = F_K\langle j\rangle$ acting on them. Second, the fluctuations around the average value $\langle j\rangle$ can be characterized by a standard deviation $\sigma_j \sim 1/\sqrt{K}$ both for the thermal and for the active process.

A comparison between Fig. 7 and 9 also shows that the tug-of-war obtained for the reduced state space with $\varepsilon_0 = 0$ is reached in a smooth manner when we consider the full state space as depicted in Fig. 4 and take the limit of small ε_0. This agreement is to be expected because the steady state probability distributions for $\varepsilon_0 > 0$ follow from the redefined network in Fig. 12 which also becomes identical with the reduced state space for $\varepsilon_0 = 0$.

3.4 Relaxation time for vanishing unbinding rate

For the reduced state space consisting of the states (j) with $j = -J,\ldots,+J$ as obtained for unbinding rate $\varepsilon_0 = 0$, the elastically coupled motors eventually reach a steady state with the average elastic force $\langle F\rangle \simeq F_{ca}$ as illustrated in Fig. 8 for $F_K = F_{ca}/8.75$. We will now address the relaxation time for this process, *i.e.* the time it takes to actually reach this steady state. This relaxation time τ_{re} is provided by the largest non-zero eigenvalue λ_2 of the transition rate matrix for the redefined state space in Fig. 12 *via* the relation[30]

$$\tau_{re} = -1/\lambda_2. \tag{3.16}$$

As shown in Fig. 11, the relaxation time τ_{re} for the approach towards the steady state increases strongly as we reduce the strain force F_K, *i.e.* as we reduce the elastic coupling between the two motors and allow them to move further apart. Indeed, in the limit of small F_K, the average separation of the two motors increases as $\langle \Delta L\rangle = \ell\langle j\rangle \sim 1/F_K$ as follows from the behavior of $\langle j\rangle$ in Fig. 10. When we plot the τ_{re}-data in a double-logarithmic manner, see the inset of Fig. 11, a least-squares fit leads to the relation $\tau_{re} \sim 1/F_K^{\eta}$ with the decay exponent $\eta = 0.97$. We thus conclude that the relaxation time τ_{re} is also inversely proportional to F_K to a very good approximation. As a consequence, the relaxation time τ_{re} for two weakly coupled motors is roughly proportional to their average separation $\langle \Delta L\rangle \sim 1/F_K$ which diverges in the limit of small $F_K = \ell\kappa/2$.

In order to obtain a well-defined relaxation time τ_{re}, we had to consider the limiting case with unbinding rate $\varepsilon_0 = 0$. Real motors have, of course, a finite unbinding rate which implies that their 2-motor runs are terminated after a finite

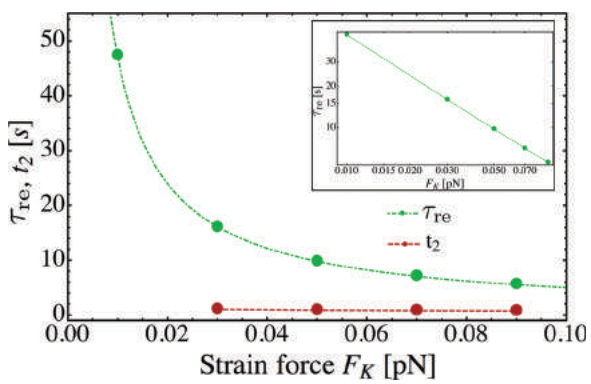

Fig. 11 Strain force dependence of the relaxation time τ_{re} (green) needed to attain the steady state for unbinding rate $\varepsilon_0 = 0$. The inset displays a double-logarithmic plot of the τ_{re}-data. A least-squares fit to these data leads to $\tau_R \sim 1/F_K^{\eta}$ with the exponent $\eta = 0.97$ from which we conclude that the relaxation time τ_{re} is inversely proportional to F_K to a very good approximation. For comparison, the average run time t_2 (red) for 2-motor runs with $\varepsilon_0 = 0.3\ s^{-1}$ has also been included. For the range of F_K-values considered here, the relaxation time τ_{re} is always large compared to the average run time t_2.

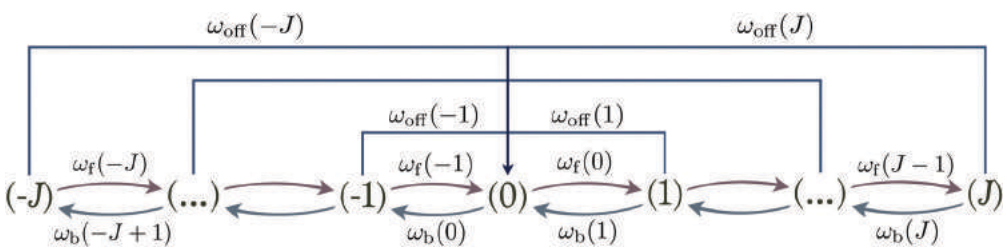

Fig. 12 Redefined state space: all transitions of the full network in Fig. 4 that reach the two absorbing states (1, +) and (1, −) are combined with a very fast rebinding transition towards the transient initial state (0). Because the rebinding process is instantaneous, the combined unbinding and rebinding transition from state (j) to state (0) is governed by the rate ω_{off} as given by eqn (2.25).

time and can then be characterized by the average run time $t_2 = \left(\sum_j p_j^{\rm st} \omega_{\rm off}(j) \right)^{-1}$. We must now distinguish different cases depending on the relative size of the average run time t_2 and the relaxation time $\tau_{\rm re}$. If t_2 is large compared to $\tau_{\rm re}$, the two motors will be characterized by an average elastic force $\langle F \rangle$ close to the cargo force $F_{\rm ca}$ of the MKL model. On the other hand, if t_2 is small compared to $\tau_{\rm re}$, the force balance between the two motors is different because $\langle F \rangle$ is small compared to $F_{\rm ca}$. As shown in Fig. 11, the latter case applies to the unbinding rate $\varepsilon_0 = 0.3\ {\rm s}^{-1}$ for the whole range of F_K-values considered in this figure. A more detailed discussion of the different timescales and the associated dynamic regimes will be given in a subsequent publication.[31]

4 Summary and outlook

In this paper, we considered the tug-of-war between one kinesin and one dynein motor, which are coupled to a common cargo *via* elastic linkers. We started from the known properties of the single motors and used these properties to derive the force-dependent stepping rates for forward and backward steps of both motors. Unexpectedly, we found that the backward stepping rate of strong dynein exhibits a maximum at an intermediate load force, see Fig. 1. We then described the elastic interaction forces between the motors and the cargo by two harmonic springs which can be combined into an effective harmonic spring between the two motors. The extension j of this effective spring was used to define the state space for the tug-of-war between two elastically coupled motors as displayed in Fig. 4.

A Markov process was constructed on this state space with transition rates that were derived from the single motor rates. Starting from the relaxed state (0) with spring extension $j = 0$, the antagonistic motors perform a 2-motor run on the reduced state space consisting of the transient states (j) with $j = -J,\ldots,+J$ until one motor unbinds from the filament and the process ends up in one of the absorbing states $(1,+)$ or $(1,-)$, see Fig. 4. The ensemble average over many such 2-motor runs can be obtained by computing the steady state probability distribution $p_j^{\rm st}$ on the redefined state space in Fig. 12. Using this distribution, we calculated the average elastic force $\langle F \rangle$ experienced by the two motors as a function of the unbinding rate ε_0, see Fig. 7. This average force approaches the cargo force $F_{\rm ca}$ for small ε_0 and decays to zero as $1/\varepsilon_0$ for large ε_0, see (3.8). Numerically we find the power law $\langle F \rangle \sim 1/\varepsilon_0^{\zeta}$ with an effective decay exponent ζ that depends on the strain force F_K, see Fig. 7(d).

Finally, we studied the limiting case of a tug-of-war between two elastically coupled motors that cannot unbind from the filament, corresponding to zero-force unbinding rate $\varepsilon_0 = 0$. In this case, we found that the time evolution of the probability distribution always leads to a steady state distribution for which (i) the average elastic force $\langle F \rangle$ is close to the cargo force $F_{\rm ca}$ irrespective of the strain force F_K and (ii) the standard deviation σ_F of the force fluctuations is proportional to $\sqrt{F_K}$ as shown in Fig. 9. These relationships imply that the average spring extension $\langle j \rangle \sim 1/F_K \sim 1/K$ and the standard deviation $\sigma_j \sim 1/\sqrt{F_K} \sim 1/\sqrt{K}$, see Fig. 10. The latter dependence is consistent with a Gaussian probability distribution for the spring extension j as described by (3.14). The behavior of the average spring extension $\langle j \rangle$ implies that the average separation $\langle \Delta L \rangle = \ell \langle j \rangle$ of the two antagonistic motors increases as $1/K$ for small K, corresponding to the weak coupling limit. Essentially the same K-dependence is found for the relaxation time $\tau_{\rm re}$ towards the steady state probability distribution $p_j^{\rm st}$, see Fig. 11. Therefore, in the weak coupling limit of small K, both the average motor separation $\langle \Delta L \rangle$ and the relaxation time $\tau_{\rm re}$ diverge as $1/K$ for $\varepsilon_0 = 0$.

In the present article, we have focussed on the forces acting between two elastically coupled motors. As indicated in the last subsection 3.4 on the relaxation time, the resulting tug-of-war involves different timescales that define different kinetic regimes. Likewise, as far as motor unbinding is concerned, one has to distinguish spontaneous unbinding for small elastic forces from force-induced unbinding for large elastic forces. Another interesting topic is the tug-of-war between elastically coupled motor teams involving $N_1 \geq 1$ plus-directed motors and $N_2 \geq 1$ minus-directed motors. These more complex motor systems will be addressed in a forthcoming paper.[31]

As previously mentioned, the theoretical results presented here can be scrutinized by experimental *in vitro* studies based on recently developed protocols[16–20] to control the number of active motors on synthetic DNA scaffolds. Evidence for a tug-of-war mechanism between kinesin and dynein attached to such scaffolds was observed in ref. 19 and 20. Very recently, it has also been demonstrated that one can directly crosslink a single, fluo-labeled kinesin with a single, fluo-labeled dynein *via* DNA hybridization.[21] Our tug-of-war model provides detailed predictions for the transport properties of such a two-motor system. One of these properties is the probability distribution $p_j^{\rm st}$ for the spatial separation of the two motors as displayed in Fig. 5a, 6a1, b1, and 8. The latter distribution should be accessible to advanced methods of fluorescence imaging such as FIONA.[29] In principle, it is also possible to measure the average interaction force $\langle F \rangle$ directly *via* FRET-based molecular tension probes[32] that are incorporated into the linkers between the motors and the cargo. Other quantities of interest that can be used to compare our theory with experiment include the run lengths and run times of the two-motor systems.

Appendices

A Review of tug-of-war with velocity matching

Here we shortly describe the tug-of-war in the MKL model, following ref. 6 and 7. Let N_+ and N_- denote the number of plus and minus motors attached to the cargo, respectively. At any given time t' the cargo is pulled by n_+ plus and n_- minus motors, where $0 \leq n_+ \leq N_+$ and $0 \leq n_- \leq N_-$. The motility state of the cargo at t' is then characterised by the

number of bound motors to the microtubule, denoted by (n_+, n_-). Assuming that (i) opposing motors act as load and (ii) identical motors share this load[6] the transition rates between adjacent motility states can be inferred from single motor binding and unbinding behaviour. The force balance on a cargo pulled by n_+ plus and n_- minus motors at any moment is given by:

$$F_{\mathrm{ca}}(n_+,n_-) \equiv n_+F^+ = -n_-F^-. \tag{A.1}$$

F^+ and F^- are the forces "felt" by a single plus and a single minus motor, respectively. The sign of the force is chosen to be positive if it is a load on the plus motors. The force acting on a single plus motor is then given by $F^+ = F_{\mathrm{ca}}(n_+,n_-)/n_+$. This means that all plus motors feel the same load in a given cargo state (n_+,n_-). The effective unbinding rate for a plus motor is:

$$\varepsilon^+(n_+,n_-) = n_+\varepsilon_0^+ \exp(|F_{\mathrm{ca}}(n_+,n_-)|/(n_+F_{\mathrm{d}}^+)). \tag{A.2}$$

Note that multiplying single motor rates by the factor n_+ implies that the motor–motor interactions are not considered. The effective binding rate of a plus motor is similarly given by:

$$\pi^+(n_+,n_-) = (N_+ - n_+)\pi_0^+. \tag{A.3}$$

The effective binding and unbinding rates for the minus motors can be obtained by replacing the index "+" by "−" in eqn (A.2) and (A.3).

An expression for the cargo force $F_{\mathrm{ca}}(n_+,n_-)$ of the force balance condition can be determined by observing that both plus and minus motor teams match their velocities under this load. The corresponding velocity is equal to the cargo velocity:

$$v_{\mathrm{ca}}(n_+,n_-) = v^+(F_{\mathrm{ca}}(n_+,n_-)/n_+) = -v^-(F_{\mathrm{ca}}(n_+,n_-)/n_-), \tag{A.4}$$

where the functions $v^+(\cdot)$ and $v^-(\cdot)$ are determined by the single plus and minus motor force–velocity relations. In ref. 6 and 7 the force–velocity relation of a single motor is given by the following piecewise-linear function:

$$v(F) = v_{\mathrm{F|B}}(1 - F/F_{\mathrm{s}}), \tag{A.5}$$

with $v_{\mathrm{F|B}} = v_{\mathrm{F}}$ for $F \le F_{\mathrm{s}}$ and $v_{\mathrm{F|B}} = v_{\mathrm{B}}$ for $F > F_{\mathrm{s}}$, where v_{F} and v_{B} are the force-free forward and backward velocity, respectively. When there is no load force acting on the motor, it proceeds with the force-free forward velocity v_{F}. Note that both v_{F} and v_{B} indicate the absolute values of the corresponding velocities. In this work, however, we use an empirical force–velocity relation obtained by a least squares fit to the data from ref. 22. This specific choice is initially presented in ref. 11, see eqn (2.1) in the main text.

From eqn (A.5) we obtain the velocity of plus motors for the state (n_+,n_-):

$$v^+(F_{\mathrm{ca}}(n_+,n_-)/n_+) = \begin{cases} v_{\mathrm{F}}^+\left(1 - F_{\mathrm{ca}}(n_+,n_-)/\left(n_+F_{\mathrm{s}}^+\right)\right), & \text{for } F_{\mathrm{ca}}(n_+,n_-) \le F_{\mathrm{s}}^+, \\ v_{\mathrm{B}}^+\left(1 - F_{\mathrm{ca}}(n_+,n_-)/\left(n_+F_{\mathrm{s}}^+\right)\right), & \text{for } F_{\mathrm{ca}}(n_+,n_-) > F_{\mathrm{s}}^+. \end{cases} \tag{A.6}$$

The minus motor velocity is given by an analogous expression by replacing the index "+" by "−". The cargo force $F_{\mathrm{ca}}(n_+,n_-)$ can now be determined by the velocity matching condition in eqn (A.4):

$$v_{\mathrm{F|B}}^+\left(1 - F_{\mathrm{ca}}(n_+,n_-)/\left(n_+F_{\mathrm{s}}^+\right)\right) = -v_{\mathrm{F|B}}^-\left(1 - F_{\mathrm{ca}}(n_+,n_-)/\left(n_-F_{\mathrm{s}}^-\right)\right),$$

$$\Leftrightarrow F_{\mathrm{ca}}(n_+,n_-) = \frac{n_+n_-F_{\mathrm{s}}^+F_{\mathrm{s}}^-\left(v_{\mathrm{F|B}}^+ + v_{\mathrm{F|B}}^-\right)}{v_{\mathrm{F|B}}^+n_-F_{\mathrm{s}}^- + v_{\mathrm{F|B}}^-n_+F_{\mathrm{s}}^+}. \tag{A.7}$$

Observe that when only one motor type is active, *i.e.* $n_- = 0$ or $n_+ = 0$, the force acting on the cargo disappears: $F_{\mathrm{ca}}(n_+,n_-) = 0$. From eqn (A.7) and (A.4), we obtain the cargo velocity:

$$v_{\mathrm{ca}}(n_+,n_-) = \frac{n_+F_{\mathrm{s}}^+ - n_-F_{\mathrm{s}}^-}{n_-F_{\mathrm{s}}^-\Big/v_{\mathrm{F|B}}^- + n_+F_{\mathrm{s}}^+\Big/v_{\mathrm{F|B}}^+}. \tag{A.8}$$

For the empirical force–velocity relationship $v(F)$ as given in the main text by eqn (2.1) the matching condition (A.4) can be solved numerically. In the case of two antagonistic motors the cargo velocity defined by the matching condition eqn (A.4) can be obtained graphically from the intersection point $(F,v) = (F_{\mathrm{ca}},v_{\mathrm{ca}})$ of two force–velocity relations, as shown in Fig. 2.

For the case of "stronger plus motors", *i.e.* $n_+F_{\mathrm{s}}^+ > n_-F_{\mathrm{s}}^-$, we have:

$$F_{\mathrm{ca}}(n_+,n_-) = \Lambda n_+F_{\mathrm{s}}^+ + (1 - \Lambda)n_-F_{\mathrm{s}}^-, \tag{A.9}$$

$$v_{\mathrm{ca}}(n_+,n_-) = \frac{n_+F_{\mathrm{s}}^+ - n_-F_{\mathrm{s}}^-}{n_-F_{\mathrm{s}}^-\Big/v_{\mathrm{B}}^- + n_+F_{\mathrm{s}}^+\Big/v_{\mathrm{F}}^+}, \tag{A.10}$$

where $\Lambda = \left(1 + \left(n_+F_{\mathrm{s}}^+v_{\mathrm{B}}^-\right)/\left(n_-F_{\mathrm{s}}^-v_{\mathrm{F}}^+\right)\right)^{-1}$. Observe that Λ can only have values in the interval [0,1], which implies that the cargo force $F_{\mathrm{ca}}(n_+,n_-)$ ranges between the maximal values of the plus and minus stall forces $n_+F_{\mathrm{s}+}$ and $n_-F_{\mathrm{s}-}$.

In this work we only consider two opposing motors, *i.e.* the state $(n_+ = 1, n_- = 1)$. The notation used in the main text is $F_{\mathrm{ca}} \equiv F_{\mathrm{ca}}(n_+ = 1, n_- = 1)$ and $v_{\mathrm{ca}} \equiv v_{\mathrm{ca}}(n_+ = 1, n_- = 1)$, where F_{ca} and v_{ca} are obtained from the numerical solution of the velocity matching condition, *i.e.* by determining the coordinates of the intersection point of the force–velocity functions of both motors.

B Master equations and the specification of parameters

The full network in Fig. 4 can be reduced to a closed network with all transitions to the two absorbing states being redirected to the initial state (0), see Fig. 12. The steady state distribution of the closed network can now be used to obtain some quantities of interest such as the average absorption time for the full network.[11,33] The latter quantity can also be calculated recursively without constructing the closed network.[34] A single trajectory on the closed network in Fig. 12 corresponds to the concatenation of many full network trajectories, each of which starts at the initial state (0) and is eventually absorbed in the

states (1, +) or (1, −). The master equations corresponding to the closed network in Fig. 12 are given by

$$\partial_t p_{-J}(t) = -[\omega_f(-J) + \omega_{off}(-J)]\, p_{-J}(t) + \omega_b(-J+1) p_{-J+1}(t) \quad \text{(B.1)}$$

and

$$\partial_t p_J(t) = -[\omega_b(J) + \omega_{off}(J)]\, p_J(t) + \omega_f(J-1) p_{J-1}(t). \quad \text{(B.2)}$$

for the two boundary states with $j = -J$ and $j = +J$, by

$$\partial_t p_0(t) = -[\omega_f(0) + \omega_b(0)] p_0(t) + \omega_b(1) p_1(t) + \omega_f(-1) p_{-1}(t) + \sum_{j\neq 0} \omega_{off}(j) p_j(t), \quad \text{(B.3)}$$

for the state (0), where the sum includes all states (j) apart from (0), and

$$\partial_t p_j(t) = -[\omega_f(j) + \omega_b(j) + \omega_{off}(j)] p_j(t) + \omega_b(j+1) p_{j+1}(t) + \omega_f(j-1) p_{j-1}(t) \quad \text{(B.4)}$$

for all other values of j. Eqn (B.1)–(B.4) are supplemented by the normalization condition

$$\sum_j p_j(t) = 1 \quad \text{for all } t. \quad \text{(B.5)}$$

The different rates that appear in these equations are defined in (2.22)–(2.25) and depend on the single motor properties described by (2.1)–(2.6). The latter relationships involve the single motor parameters v_0, v_{max}, v_{min}, F_s, q_0, F_d, ε_0, and ℓ as well as the elastic coupling parameter $K = \kappa/2$. We typically vary one parameter such as the unbinding rate ε_0 or the elastic coupling parameter K, keeping all other parameters fixed at their values in Table 1.

C Matrix form of master equations

The master equations can be written in the matrix form if we define the $(2J+1)$-dimensional column vector

$$(p_{-J}(t), p_{-J+1}(t), \ldots, p_{J-1}(t), p_J(t))^T \equiv |p(t)\rangle \quad \text{(C.1)}$$

where the superscript T stands for 'transpose' and the ket notation will be used for convenience. Using the latter vector, the master equations (B.1)–(B.4) attain the compact form

$$\partial_t |p(t)\rangle = \mathbf{W} |p(t)\rangle \quad \text{(C.2)}$$

with the $(2J+1) \times (2J+1)$ transition rate matrix $\mathbf{W}$. The diagonal matrix elements $W_{j,j}$ are given by

$$W_{j,j} = -[\omega_f(j) + \omega_b(j) + \omega_{off}(j)] \quad \text{for } j \neq -J, j \neq 0, \text{ and } j \neq J \quad \text{(C.3)}$$

as well as by

$$W_{-J,-J} = -[\omega_f(-J) + \omega_{off}(-J)], \quad \text{(C.4)}$$

$$W_{0,0} = -[\omega_f(0) + \omega_b(0)], \quad \text{(C.5)}$$

and

$$W_{J,J} = -[\omega_b(J) + \omega_{off}(J)]. \quad \text{(C.6)}$$

The off-diagonal matrix elements of $\mathbf{W}$ are given by

$$W_{j,j+1} = \omega_b(j+1) \quad \text{for } j \leq J-1 \quad \text{(C.7)}$$

and

$$W_{j,j-1} = \omega_f(j-1) \quad \text{for } j \geq -J+1. \quad \text{(C.8)}$$

For each column of the matrix $\mathbf{W}$, the matrix elements sum up to zero, *i.e.* $\sum_j W_{j,k} = 0$ for all values of k.

Most of our results are based on the steady state solutions p_j^{st} of eqn (C.2) with $\partial_t |p^{st}\rangle = \mathbf{W}|p^{st}\rangle = 0$ or

$$\sum_k W_{j,k} p_k^{st} = \lambda_1 p_j^{st} \quad \text{with eigenvalue } \lambda_1 = 0. \quad \text{(C.9)}$$

The numerical solutions of these equations were obtained with a self-written script based on built-in subroutines of *Mathematica 9.0*.

D Time evolution without motor unbinding

In Section 3.3, we describe the time evolution of the probability distribution $p_j(t)$ for unbinding rate $\varepsilon_0 = 0$, see Fig. 8. In this limiting case, the state space in Fig. 4 becomes 1-dimensional and does not contain any cycles. The steady state probability distribution p_j^{st} then satisfies the detailed balance conditions

$$\omega_f(j-1) p_{j-1}^{st} - \omega_b(j) p_j^{st} = W_{j,j-1} p_{j-1}^{st} - W_{j-1,j} p_j^{st} = 0 \quad \text{(D.1)}$$

for all j with $-J \leq j \leq J-1$ which is equivalent to

$$W_{i,j} p_j^{st} = W_{j,i} p_i^{st} \quad \text{(D.2)}$$

for all nonzero matrix elements. Applying the conditions (D.1) iteratively along the 1-dimensional state space, we obtain the steady state solutions

$$p_j^{st} = \frac{\omega_f(j-1)\omega_f(j-2)\cdots\omega_f(-J+1)\omega_f(-J)}{\omega_b(j)\omega_b(j-1)\cdots\omega_b(-J+2)\omega_b(-J+1)} p_{-J}^{st}, \quad \text{(D.3)}$$

where p_{-J}^{st} is determined by the normalization condition $\sum_j p_j^{st} = 1$.

In general, the matrix $\mathbf{W}$ is not symmetric. However, if the matrix elements $W_{i,j}$ fulfill the detailed balance conditions (D.2), we can define the symmetric transition rate matrix $\tilde{\mathbf{W}}$ with matrix elements[41]

$$\tilde{W}_{j,k} \equiv W_{j,k} \left(\frac{p_k^{st}}{p_j^{st}}\right)^{1/2} = \tilde{W}_{k,j}. \quad \text{(D.4)}$$

Because the matrix $\tilde{\mathbf{W}}$ is symmetric, it has real eigenvalues λ_n with $n = 1,2,\ldots,N$ and $N = 2J+1$. Furthermore, the right and left eigenvectors for the eigenvalue λ_n have the same components $\tilde{u}_j(\lambda_n)$, *i.e.*

$$\sum_k \tilde{W}_{j,k} \tilde{u}_k(\lambda_n) = \lambda_n \tilde{u}_j(\lambda_n) \quad \text{and} \quad \sum_j \tilde{u}_j(\lambda_n) \tilde{W}_{j,k} = \lambda_n \tilde{u}_k(\lambda_n) \quad \text{(D.5)}$$

and satisfy the orthonormality condition

$$\sum_j \tilde{u}_j(\lambda_m) \tilde{u}_j(\lambda_n) = \delta_{m,n} \quad \text{(D.6)}$$

where the Kronecker delta symbol $\delta_{m,n} = 1$ for $m = n$ and 0 otherwise.

It then follows from eqn (D.4) that the transition rate matrix $\mathbf{W}$ has the same eigenvalues λ_n as the symmetric matrix $\tilde{\mathbf{W}}$ and that the right eigenvectors of $\mathbf{W}$ are given by the column vectors

$$|\lambda_n\rangle = (r_1(\lambda_n), \ldots, r_N(\lambda_n))^{\mathrm{T}} \quad \text{with } r_j(\lambda_n) \equiv \tilde{u}_j(\lambda_n)\sqrt{p_j^{\mathrm{st}}} \quad \text{(D.7)}$$

whereas the left eigenvectors of $\mathbf{W}$ are provided by the row vector

$$\langle\lambda_n| = (\ell_1(\lambda_n), \ldots, \ell_N(\lambda_n)) \quad \text{with } \ell_j(\lambda_n) \equiv \frac{\tilde{u}_j(\lambda_n)}{\sqrt{p_j^{\mathrm{st}}}}. \quad \text{(D.8)}$$

The left and right eigenvectors satisfy the orthonormality and completeness relations

$$\langle\lambda_m \mid \lambda_n\rangle = \delta_{m,n} \quad \text{and} \quad \sum_n |\lambda_n\rangle\langle\lambda_n| = \mathbf{1} \quad \text{(D.9)}$$

with the identity matrix $\mathbf{1}$. The column vector $|p(t)\rangle$ can now be decomposed according to

$$|p(t)\rangle = \sum_n |\lambda_n\rangle C_n(t) \quad \text{with } C_n(t) \equiv \langle\lambda_n \mid p(t)\rangle. \quad \text{(D.10)}$$

When this decomposition is inserted into the master equation (C.2), we obtain the time-dependent coefficients $C_n(t) = C_n(0)\mathrm{e}^{\lambda_n t}$ and the probabilities

$$p_j(t) = \sqrt{p_j^{\mathrm{st}}} \sum_n \tilde{u}_j(\lambda_n) C_n(0) \mathrm{e}^{\lambda_n t} \quad \text{(D.11)}$$

with

$$C_n(0) = \sum_k \frac{\tilde{u}_k(\lambda_n)}{\sqrt{p_k^{\mathrm{st}}}} p_k(0). \quad \text{(D.12)}$$

Because all eigenvalues λ_n are negative for $n \geq 2$, the long time behavior of $p_j(t)$ is dominated by the term with $n = 1$ and $\lambda_1 = 0$ corresponding to the steady state probabilities p_j^{st}.

Thus, in order to determine the time-dependent probabilites $p_j(t)$ as given by (D.11), we subsequently computed the steady state probabilities p_j^{st}, see (D.3), the symmetric matrix $\tilde{\mathbf{W}}$ *via* (D.4), as well as the eigenvalues λ_n of $\tilde{\mathbf{W}}$ and the corresponding eigenvectors with components $\tilde{u}_j(\lambda_n)$, using again the built-in subroutines of *Mathematica 9.0*. The initial distributions were set to $p_j(t = 0) = 1$ for $j = 0$ and $p_j(t = 0) = 0$ for all other values of j.

E Dependence of average elastic force on strain force

In Fig. 9 the strain force dependency of the average elastic force $\langle F\rangle$ is presented up to a strain force value of $F_K \simeq 3$ pN. In this regime, the average elastic force is approximately independent of the strain force and equal to the cargo force F_{ca} of the tug-of-war in the MKL model. In the limit of high strain forces, however, we would expect the elastically coupled model to generate $\langle F\rangle = 0$, since none of the motors would be able to make a single step because of the high spring stiffness.

In Fig. 13 we plot the average force $\langle F\rangle$ as a function of the strain force F_K within the range 3 pN $\leq F_K \leq$ 40 pN. We observe a weak maximum of $\langle F\rangle$ around a strain force value of $F_K \simeq 10$ pN.

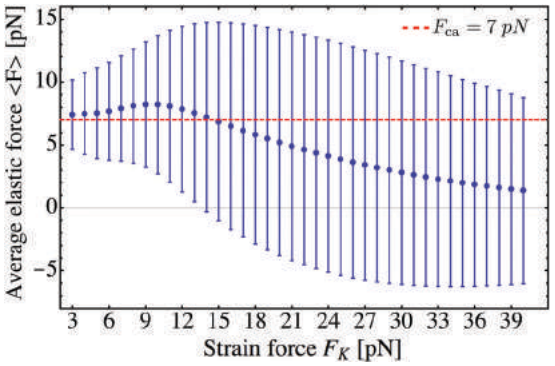

Fig. 13 Average elastic force $\langle F\rangle$ of the process for zero-force unbinding rate $\varepsilon_0 = 0$ and strain forces $F_K \geq 3$ pN. We observe that $\langle F\rangle$ reaches a maximum around a strain force value of $F_K = 10$ pN. For larger strain forces corresponding to stiffer springs, the average force $\langle F\rangle$ induced by the motors decreases monotonically to zero.

For $F_K \geq 15$ pN, the average force $\langle F\rangle$ decreases monotonically towards zero. Considering the steady state distribution over the discrete state space one can interpret the F_K-dependence of $\langle F\rangle$ as follows. Up to a strain force value of $F_K \simeq 2F_{\mathrm{s}}^{+} = 2F_{\mathrm{s}}^{-}$ the process can perform at least one step resulting in a stretching of the linker between the motors. Recall that the transition from state (0) to state (1) occurs with the sum of forward stepping rates $\alpha^{+}(\bar{F}_{0>}) + \alpha^{-}(\bar{F}_{0>})$, see eqn (2.22), where the motors feel the effective force $\bar{F}_{0>} = F_K/2$. For a strain force of $F_K = 14$ pN this force is $\bar{F}_{0>} = 7$ pN $= F_{\mathrm{s}}^{+} = F_{\mathrm{s}}^{-}$, at which the motors are equally likely to perform a forward or a backward step. Without motor unbinding, and taking into account that a further transition from (1) to (2) with an effective force of $\bar{F}_{1>} = 14$ pN acting on the motors is highly unlikely, this force balance is expected to lead to steady state probabilities $p_0^{\mathrm{st}} \simeq p_1^{\mathrm{st}} \simeq 0.5$ and to the average elastic force $\langle F\rangle \simeq p_0^{\mathrm{st}}F_0 + p_1^{\mathrm{st}}F_1 = 7$ pN $= F_{\mathrm{ca}}$.† A further increase in the strain force F_K shifts the steady state distribution towards the relaxed state (0), *i.e.* $p_0^{\mathrm{st}} > p_1^{\mathrm{st}}$, resulting in a reduction of the average force $\langle F\rangle$ towards zero. The initial increase of $\langle F\rangle$ with increasing F_K implies that the corresponding increase in F_1 overcompensates the decrease of p_1^{st} for $F_K < 10$ pN, see the steady state distribution in Fig. 14.

In Fig. 14 we plot the time evolution of the probability distribution over the states $p_j(t)$ starting from an initial state different from (0). We fix a high strain force $F_K = 10$ pN, corresponding to the maximum of $\langle F\rangle$ in Fig. 13, and choose the initial state to be (5), *i.e.* $p_j(0) = \delta_{j5}$. As t increases we see that the time-dependent probability distribution $p_j(t)$ approaches the steady state distribution p_j^{st} (dashed red line). We see that p_j^{st} has a clear peak in state (1), but also a nonzero value in (2), where the corresponding elastic force is given by $F_2 = 2F_K = 20$ pN. These high force value contributions from state (2) to the average force results in $\langle F\rangle > F_{\mathrm{ca}}$, as observed in Fig. 13.

† In this discussion we ignore the backward transitions (0) → (−1) leading to a compression of the spring, since the transition rate for (0) → (−1) is much smaller than the rate for (−1) → (0), *e.g.* for a strain force of $F_K = 14$ pN we would have $\omega_{\mathrm{f}}(-1) \simeq 10\omega_{\mathrm{b}}(0)$.

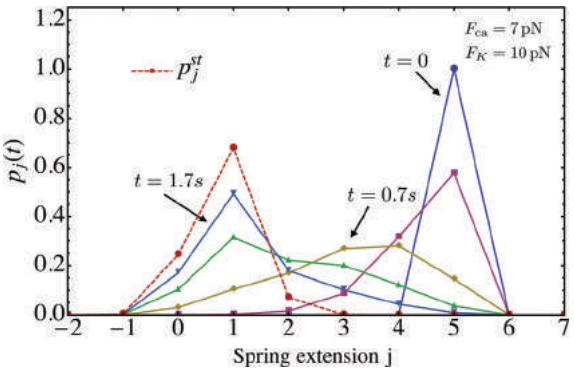

Fig. 14 Time evolution of the probability distribution $p_j(t)$ for a strain force of F_K = 10 pN. The initial probability distribution is $p_j(0) = \delta_{j5}$. The probability distribution $p_j(t)$ approaches the steady state distribution p_j^{st}, indicated by the dashed red line, which has a maximum for spring extension j = 1.

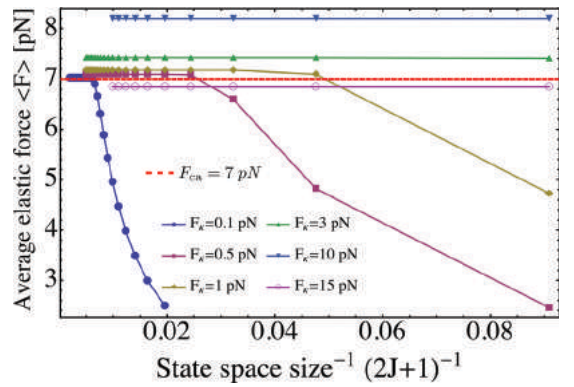

Fig. 15 Dependence of average elastic force $\langle F\rangle$ on the inverse size $(2J+1)^{-1}$ of the state space. If the two motors are weakly coupled, the finite size of the state space acts to truncate the probability distributions. Thus, for F_K = 0.1 pN, we see large finite size effects and a strong decay of $\langle F\rangle$ already for $(2J+1)^{-1} \gtrsim 0.005$.

F Dependence of force distribution on the size of state space

As shown in Fig. 10, the probability distribution p_j^{st} is shifted towards larger j-values and becomes broader as we decrease the strain force F_K. Therefore, a fixed size of the state space, *i.e.* a fixed number $(2J+1)$ of states, acts to truncate the distribution p_j^{st} for sufficiently small values of F_K. Likewise, the average elastic force $\langle F\rangle$ starts to decrease, for a fixed value of F_K, as we decrease the size $(2J+1)$ of the state space below a certain minimal value.

These finite size effects are illustrated in Fig. 15 where the average elastic force $\langle F\rangle$ is plotted as a function of the inverse size $(2J+1)^{-1}$ of the state space. Inspection of this figure shows that $\langle F\rangle$ attains a constant value for sufficiently small $(2J+1)^{-1}$ but decays strongly for sufficiently large $(2J+1)^{-1}$. In practice, we chose $(2J+1) \geq 201$ for $F_K \leq 0.1$ pN and $(2J+1) \geq 51$ for $F_K \leq 0.5$ pN.

Glossary of mathematical symbols

$\alpha(F)$	Force-dependent forward stepping rate
$\beta(F)$	Force-dependent backward stepping rate
δ_{ij}	Kronecker delta symbol
ε_0	Zero-force unbinding rate
$\varepsilon(F)$	Force-dependent unbinding rate
ζ	Effective decay exponent in $\langle F\rangle \sim \varepsilon_0^{-\zeta}$, see Fig. 7
η	Decay exponent in $\tau_{re} \sim F_K^{-\eta}$, see Fig. 11
F_{ca}	Cargo force of the MKL model
F_d	Detachment force
F_s	Stall force
$F_{dy,ca}$	Force exerted by the dynein motor onto the cargo
$F_{ki,ca}$	Force exerted by the kinesin motor onto the cargo
F_j	Elastic force acting in state (j), defined by $F_j \equiv jF_K$
$\bar{F}_{j>}$	Effective force acting during the stretching by a single step
$\bar{F}_{j<}$	Effective force acting during the compression by a single step
F_K	Effective strain force, $F_K = K\ell$
$F^{\pm}$	Force acting on single plus/minus motors in the MKL model
j	Integer spring extension in units of ℓ, $-J \leq j \leq J$
(j)	State corresponding to the spring extension j
J	Maximal value of j
κ	Spring constant of a single motor linker
K	Effective spring constant, $K = \kappa/2$,
k_B	Boltzmann constant
ℓ	Step size of the motors
$L_{\|}$	Rest length of a single elastic linker
L_0	Effective rest length of two elastic linkers, $L_0 = 2L_{\|}$
ΔL	Extension of the effective spring
λ_n	Eigenvalue of the transition rate matrix $\mathbf{W}$
$N_{\pm}$	Number of plus/minus motors attached to the cargo
$n_{\pm}$	Number of active motors bound to the filament
$\omega_f(j)$	Forward transition rate
$\omega_b(j)$	Backward transition rate
$\omega_{off}(j)$	Overall unbinding rate
p_j^{eq}	Equilibrium probability to be in state (j), see eqn (3.15)
p_j^{st}	Steady state probability to be in state (j)
$p_j(t)$	Time-dependent probability to be in state (j)
q_0	Zero-force forward-to-backward stepping ratio
$q(F)$	Force-dependent forward-to-backward stepping ratio
σ_F	Standard deviation of the force distribution
σ_j	Standard deviation of the probability distribution p_j^{st}
τ_{re}	Relaxation time
t_2	Average two-motor binding time
$\|\lambda_n\rangle$	Right eigenvector of $\mathbf{W}$ for eigenvalue λ_n
$\langle\lambda_n\|$	Left eigenvector of $\mathbf{W}$ for eigenvalue λ_n
v_{ca}	Cargo velocity of the velocity-matched state
v_0	Zero-force velocity
v_{max}	Maximal forward velocity
v_{min}	Backward velocity
v_F	Force-free forward velocity of the MKL model
v_B	Force-free backward velocity of the MKL model
$v_{F\|B}$	Velocity parameter given by v_F or v_B

$\mathbf{W}$	Transition rate matrix of the redefined state space in Fig. 12
$W_{i,j}$	$(2J+1) \times (2J+1)$ matrix elements of $\mathbf{W}$
$\tilde{\mathbf{W}}$	Symmetric transition rate matrix as defined by eqn (D.4)
$\tilde{W}_{i,j}$	$(2J+1) \times (2J+1)$ matrix elements of $\tilde{\mathbf{W}}$
x_{ki}	Position of the kinesin motor
x_{dy}	Position of the dynein motor
x_{ca}	Position of the cargo

References

1 H. Lodish, A. Berk and S. L. Zipursky, *et al*. Molecular Cell Biology, W. H. Freeman, New York, 4th edn, 2000.

2 J. Howard, *Mechanics of Motor Proteins and the Cytoskeleton*, Palgrave Macmillan, Sunderland, MA, 2005.

3 R. D. Vale, The Molecular Motor Toolbox for Intracellular Transport, *Cell*, 2003, **112**, 467–480.

4 M. A. Welte and S. P. Gross, Molecular motors: a traffic cop within?, *HFSP J.*, 2008, **2**, 178–182.

5 B. H. Blehm and P. R. Selvin, Single-molecule fluorescence and in vivo optical traps: how multiple dyneins and kinesins interact, *Chem. Rev.*, 2014, **114**(6), 3335–3352.

6 M. J. Müller, S. Klumpp and R. Lipowsky, Tug-of-war as a cooperative mechanism for bidirectional cargo transport by molecular motors, *Proc. Natl. Acad. Sci. U. S. A.*, 2008, **105**(12), 4609–4614.

7 M. J. Müller, S. Klumpp and R. Lipowsky, Motility states of molecular motors engaged in a stochastic tug-of-war, *J. Stat. Phys.*, 2008, **133**(6), 1059–1081.

8 R. Lipowsky, J. Beeg, R. Dimova, S. Klumpp and M. J. I. Müller, Cooperative behavior of molecular motors: cargo transport and traffic phenomena, *Physica E.*, 2010, **42**(3), 649–661.

9 V. Soppina, A. K. Rai, A. J. Ramaiya, P. Barak and R. Mallik, Tug-of-war between dissimilar teams of microtubule motors regulates transport and fission of endosomes, *Proc. Natl. Acad. Sci. U. S. A.*, 2009, **106**(46), 19381–19386.

10 M. Schuster, R. Lipowsky, M. A. Assmann, P. Lenz and G. Steinberg, Transient binding of dynein controls bidirectional long-range motility of early endosomes, *Proc. Natl. Acad. Sci. U. S. A.*, 2011, **108**(9), 3618–3623.

11 F. Berger, C. Keller, S. Klumpp and R. Lipowsky, Distinct transport regimes for two elastically coupled molecular motors, *Phys. Rev. Lett.*, 2012, **108**(20), 208101.

12 F. Berger, C. Keller, S. Klumpp and R. Lipowsky, External forces influence the elastic coupling effects during cargo transport by molecular motors, *Phys. Rev. E: Stat., Nonlinear, Soft Matter Phys.*, 2015, **91**(2), 022701.

13 A. Kunwar and A. Mogilner, Robust transport by multiple motors with nonlinear force–velocity relations and stochastic load sharing, *Phys. Biol.*, 2010, **7**(1), 016012.

14 A. Kunwar, S. K. Tripathy, J. Xu, M. K. Mattson, P. Anand and R. Sigua, *et al.* Mechanical stochastic tug-of-war models cannot explain bidirectional lipid-droplet transport, *Proc. Natl. Acad. Sci. U. S. A.*, 2011, **108**(47), 18960–18965.

15 S. Klein, C. Appert-Rolland and L. Santen, Motility states in bidirectional cargo transport, *EPL*, 2015, **111**(6), 68005.

16 D. K. Jamison, J. W. Driver, A. R. Rogers, P. E. Constantinou and M. R. Diehl, Two kinesins transport cargo primarily via the action of one motor: implications for intracellular transport, *Biophys. J.*, 2010, **99**(9), 2967–2977.

17 A. R. Rogers, J. W. Driver, P. E. Constantinou, D. K. Jamison and M. R. Diehl, Negative interference dominates collective transport of kinesin motors in the absence of load, *Phys. Chem. Chem. Phys.*, 2009, **11**(24), 4882–4889.

18 H. Lu, A. K. Efremov, C. S. Bookwalter, E. B. Krementsova, J. W. Driver and K. M. Trybus, *et al.* Collective dynamics of elastically coupled myosin V motors, *J. Biol. Chem.*, 2012, **287**(33), 27753–27761.

19 K. Furuta, A. Furuta, Y. Y. Toyoshima, M. Amino, K. Oiwa and H. Kojima, Measuring collective transport by defined numbers of processive and nonprocessive kinesin motors, *Proc. Natl. Acad. Sci. U. S. A.*, 2013, **110**(2), 501–506.

20 N. D. Derr, B. S. Goodman, R. Jungmann, A. E. Leschziner, W. M. Shih and S. L. Reck-Peterson, Tug-of-war in motor protein ensembles revealed with a programmable DNA origami scaffold, *Science*, 2012, **338**(6107), 662–665.

21 V. Belyy, M. A. Schlager, H. Foster, A. E. Reimer, A. P. Carter and A. Yildiz, The mammalian dynein-dynactin complex is a strong opponent to kinesin in a tug-of-war competition, *Nat. Cell Biol.*, 2016, **18**, 1018–1024.

22 N. J. Carter and R. Cross, Mechanics of the kinesin step, *Nature*, 2005, **435**(7040), 308–312.

23 M. Nishiyama, H. Higuchi and T. Yanagida, Chemomechanical coupling of the forward and backward steps of single kinesin molecules, *Nat. Cell Biol.*, 2002, **4**(10), 790–797.

24 S. Toba, T. M. Watanabe, L. Yamaguchi-Okimoto, Y. Y. Toyoshima and H. Higuchi, Overlapping hand-over-hand mechanism of single molecular motility of cytoplasmic dynein, *Proc. Natl. Acad. Sci. U. S. A.*, 2006, **103**(15), 5741–5745.

25 S. L. Reck-Peterson, A. Yildiz, A. P. Carter, A. Gennerich, N. Zhang and R. D. Vale, Single-molecule analysis of dynein processivity and stepping behavior, *Cell*, 2006, **126**(2), 335–348.

26 A. Gennerich, A. P. Carter, S. L. Reck-Peterson and R. D. Vale, Force-induced bidirectional stepping of cytoplasmic dynein, *Cell*, 2007, **131**(5), 952–965.

27 M. Plischke and B. Bergersen, *Equilibrium statistical physics*, World Scientific, 2006.

28 C. Keller, R. Lipowsky, unpublished.

29 A. Yildiz and P. R. Selvin, Fluorescence Imaging with One Nanometer Accuracy: Application to Molecular Motors, *Acc. Chem. Res.*, 2005, **38**, 574–582.

30 M. Kijima, *Markov processes for stochastic modeling*, CRC Press, 1997, vol. 6.

31 M. C. Ucar, R. Lipowsky, unpublished.

32 C. Gayrard and N. Borghi, FRET-based Molecular Tension Microscopy, *Methods*, 2016, **94**, 33–42.

33 T. L. Hill, Interrelations between random walks on diagrams (graphs) with and without cycles, *Proc. Natl. Acad. Sci. U. S. A.*, 1988, **85**(9), 2879–2883.

34 J. R. Norris, *Markov chains*, Cambridge University Press, 1998, vol. 2.
35 R. D. Vale, T. Funatsu, D. W. Pierce, L. Romberg, Y. Harada and T. Yanagida, Direct observation of single kinesin molecules moving along microtubules, *Nature*, 1996, **380**(6573), 451–453.
36 S. J. King and T. A. Schroer, Dynactin increases the processivity of the cytoplasmic dynein motor, *Nat. Cell Biol.*, 2000, **2**(1), 20–24.
37 A. K. Rai, A. Rai, A. J. Ramaiya, R. Jha and R. Mallik, Molecular adaptations allow dynein to generate large collective forces inside cells, *Cell*, 2013, **152**(1), 172–182.
38 B. H. Blehm, T. A. Schroer, K. M. Trybus, Y. R. Chemla and P. R. Selvin, In vivo optical trapping indicates kinesin's stall force is reduced by dynein during intracellular transport, *Proc. Natl. Acad. Sci. U. S. A.*, 2013, **110**(9), 3381–3386.
39 S. Uemura, K. Kawaguchi, J. Yajima, M. Edamatsu, Y. Y. Toyoshima and S. Ishiwata, Kinesin-microtubule binding depends on both nucleotide state and loading direction, *Proc. Natl. Acad. Sci. U. S. A.*, 2002, **99**(9), 5977–5981.
40 M. P. Nicholas, F. Berger, L. Rao, S. Brenner, C. Cho and A. Gennerich, Cytoplasmic dynein regulates its attachment to microtubules *via* nucleotide state-switched mechanosensing at multiple AAA domains, *Proc. Natl. Acad. Sci. U. S. A.*, 2015, **112**(20), 6371–6376.
41 N. G. Van Kampen, *Stochastic processes in physics and chemistry*, Elsevier, 1992, vol. 1.

